Available online at www.sciencedirect.com
SCIENCE DIRECT®
Journal of Sound and Vibration 280 (2005) 235–262
JOURNAL OF SOUND AND VIBRATION
www.elsevier.com/locate/jsvi

Vibration localization in plates rib-stiffened in two orthogonal directions

Z. Chen, W.-C. Xie*

Solid Mechanics Division, Faculty of Engineering, University of Waterloo, Waterloo, Ont., Canada N2L 3G1

Received 6 September 2002; accepted 4 December 2003

Abstract

This study deals with the vibration localization in plates rib-stiffened in two orthogonal directions. The effect of small misplacements of stiffeners, with various combinations of flexural and torsional rigidities, on both the free vibration modes and forced vibration responses of a plate clamped at four edges is presented. An extended finite strip approach, or the compound strip method, is employed to obtain the natural frequencies and the corresponding vibration modes. Galerkin's method is applied to determine the forced vibration response of the rib-stiffened plate subjected to a harmonic concentrated load at the center of one of its four panels. It is observed that a small disorder of the rib-stiffeners may significantly affect the vibration localization of the whole plate. By deliberately introducing irregularity into the stiffeners, the vibration magnitudes of some of the panels of the plate may be reduced.

1. Introduction

It is well known that small deviations of periodicity in large periodic engineering structures, such as stiffened plates, have dramatic effects on their dynamical properties and lead to the localization of vibration, in which vibration is confined in a small region close to the source of vibration. Furthermore, a periodic structure may be purposely disordered so that the localization behavior can be used to serve as a damping mechanism. Although disorder and dissipation both result in a spatial decay of the amplitude, the localization and damping mechanisms are intrinsically distinct. For localization the vibration energy is confined in a small

*Corresponding author. Tel.: +1-519-888-4567; fax: +1-519-888-6197.
E-mail address: xie@uwaterloo.ca (W.-C. Xie).

0022-460X/$ - see front matter
doi:10.1016/j.jsv.2003.12.029

region near the source of excitation by disorder, while for damping the energy is dissipated as it propagates.

Localization phenomenon was first discovered by P.W. Anderson in 1958 in the field of solid state physics. The study of its occurrence has been investigated by many researchers during the past four decades. The first known research on localization phenomenon in the area of structural dynamics was done by Hodges [1], who evidenced this phenomenon in structural dynamics by both theoretical investigation and experimental demonstration [2]. Since then, the problem of localization has stimulated a number of structural dynamicists. A detailed review on vibration localization can be found in Ref. [3] and in the papers in the special issue on ''Localization in Engineering Problems'' [4].

The localization phenomenon in disordered engineering structures can have either beneficial or harmful effects.

Localization of vibration is important because the dynamic response of a disordered system may be considerably higher than that of a perfect system, leading to higher vibration levels and larger stresses. It has been found that the small differences in the structural or inertial properties of a structure can affect the amplitudes of individual substructures by several hundred percent, which can result in structural failure [5]. Since localization occurs even for small deviations of periodicity in the structure, prediction of the response of a disordered structure is particularly important. In fact, disorder played an important role in several costly failures in the development and production of modern aircraft turbofan engines [6]. In these cases, vibration localization has a detrimental effect on the performance of the structures.

In the *Steel Design Guide Series 11: Floor Vibrations Due to Human Activity* by the American Institute of Steel Construction [7], the following problem is described. Extremely annoying floor vibrations sometimes occur in large open floor areas where the floor is supported by identical, equally and closely spaced joists and beams. The sensation is ''wave-like'' with waves rolling back and forth across the width of the building. Also, because of the transmission of the vibration, an occupant who is unaware of the cause of the motion is suddenly subjected to significant motion and may be particularly annoyed. Vibration transmission of this type can be reduced, if not eliminated, by changing the stiffness of some of the joist members, say at the column lines, or by changing the spacing in alternate bays.

Although the design guide did not identify this as a localization problem and only provided solutions from experience, this is actually an example in which localization in vibration propagation is beneficial. By purposely interrupting the periodicity of the floor system, the amplitudes of propagating waves due to impact will be localized in the vicinity of the point of impact or the amplitudes of vibration will decay exponentially from the point of impact.

In this paper, the vibration localization of plates with intermediate rib-stiffeners in two orthogonal directions is investigated. The dynamic response of such plates under harmonic excitation is of great importance in various engineering structures such as ship superstructures, bridge decks, ribbed floors, aircraft, and space structures.

Generally, studies of dynamic behavior of stiffened plates may be classified into two approaches. One basic approach is to represent the stiffened plate by an equivalent orthotropic plate of constant thickness having the same stiffness characteristics. However, the actual structural behavior of the stiffened plate cannot be completely replaced by that of an orthotropic plate. When the stiffeners have different cross-section properties or are unequally spaced, which

is of the case of the current study, the orthotropic plate idealization is no longer applicable. Furthermore, this approach cannot be expected to yield good results for cases with large stiffener spacings.

Another more realistic approach treats the contribution of the plate and stiffeners separately, see, e.g., Ref. [8], in which the free and forced vibrations of elastically cross-supported rectangular plates with viscoelastic edge conditions were considered. However, the formulation presented in Ref. [8] is not applicable to plate with rib-stiffeners, since a rib-stiffened plate differs from a spring-supported plate by the fact that the rib-stiffeners have mass while the springs do not.

On the other hand, applying compound strip method [9] and Galerkin's method to study vibration localization of these plates is simple, less demanding on computer time, and can be easily formulated. Since building floors may be modelled as plates stiffened in two orthogonal directions, it is important to study in detail the vibration behavior of disordered plates with intermediate stiffeners. The current approach emphasizes the effect of misplacements of stiffeners on vibration response, i.e., vibration localization.

2. Vibration mode localization by the compound strip method

2.1. Assembly of stiffness and mass matrices

Consider a uniform rectangular plate of length L, width b, and thickness h, which is stiffened by two intermediate rib-stiffeners in two orthogonal directions as shown in Fig. 1. Suppose the plate is clamped at its four edges without loss of generality. An extended finite strip method, the compound strip method, is employed to study the free vibration of the four-panel plate. For completeness of the paper, an introduction to the compound strip method is given in Appendix A.

Each span of the stiffened plate in the x direction is divided into M strips of equal width as shown in Fig. 2, i.e., for Span 1 of width L_1, $l_{11} = l_{12} = \cdots = l_{1M} = L_1/M$, and for Span 2 of width L_2, $l_{21} = l_{22} = \cdots = l_{2M} = L_2/M$, where l_{ij} denotes the width of the jth strip of the ith span.

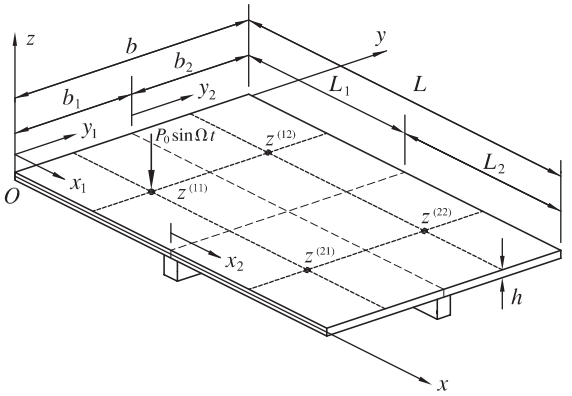

Fig. 1. A four-panel rectangular plate.

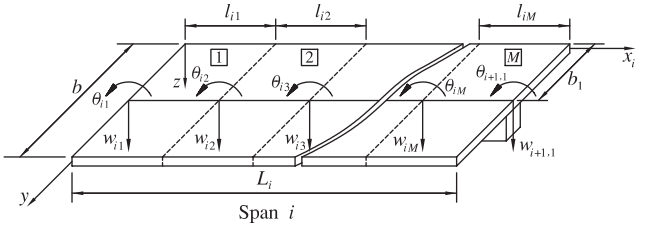

Fig. 2. Finite strip discretization of the ith span.

It is well known that the dynamic equilibrium equation of any linear elastic structure in free vibration is given by $(\mathbf{K}-\omega^2\mathbf{M})\mathbf{u}=0$, where ω is the natural frequency, $\mathbf{K}$ is the overall stiffness matrix of the structure, $\mathbf{M}$ is the overall mass matrix, and $\mathbf{u}$ is the nodal displacement vector.

Assembling the non-dimensional stiffness and the mass matrices for the whole plate shown in Fig. 1, the non-dimensional equations of motion are given by

$$(\hat{\mathbf{K}}-\mu\hat{\mathbf{M}})\hat{\mathbf{u}}=\mathbf{0}, \tag{1}$$

where μ is the non-dimensional frequency of the plate defined in Eqs. (A.3) in Appendix A. The non-dimensional overall stiffness matrix is given by

$$\hat{\mathbf{K}}=\begin{bmatrix}
[\hat{\mathbf{K}}_{11}]^{11} & [\hat{\mathbf{K}}_{12}]^{11} & & & & & & & & \\
[\hat{\mathbf{K}}_{21}]^{11} & [\hat{\mathbf{K}}]^{12} & [\hat{\mathbf{K}}_{12}]^{12} & & & & & & & \\
 & \ddots & \ddots & \ddots & & & & & & \\
 & & [\hat{\mathbf{K}}_{21}]^{1(N-1)} & [\hat{\mathbf{K}}]^{1N} & [\hat{\mathbf{K}}_{12}]^{1N} & & & & & \\
 & & & [\hat{\mathbf{K}}_{21}]^{1N} & [\hat{\mathbf{K}}_c]^{21} & [\hat{\mathbf{K}}_{12}]^{21} & & & & \\
 & & & & [\hat{\mathbf{K}}_{21}]^{21} & [\hat{\mathbf{K}}]^{22} & [\hat{\mathbf{K}}_{12}]^{22} & & & \\
 & & & & & \ddots & \ddots & \ddots & & \\
 & & & & & & [\hat{\mathbf{K}}_{21}]^{2(N-1)} & [\hat{\mathbf{K}}]^{2N} & [\hat{\mathbf{K}}_{12}]^{2N} \\
 & & & & & & & [\hat{\mathbf{K}}_{21}]^{2N} & [\hat{\mathbf{K}}_{22}]^{2N}
\end{bmatrix},$$

in which, for $i=1,2$, $j=1,2,\ldots,N$,

$$[\hat{\mathbf{K}}]^{ij}=[\hat{\mathbf{K}}_{22}]^{i(j-1)}+[\hat{\mathbf{K}}_{11}]^{ij},\quad [\hat{\mathbf{K}}_{\mathrm{c}}]^{21}=[\hat{\mathbf{K}}_{22}]^{1N}+[\hat{\mathbf{K}}_{11}]^{21}+[{}^{LS}\hat{\mathbf{K}}]^{21}_{11},$$

where

$$[\hat{\mathbf{K}}_{pq}]^{ij}=\begin{bmatrix}
[\hat{\mathbf{K}}_{pq}]^{ij}_{11} & [\hat{\mathbf{K}}_{pq}]^{ij}_{12} & \cdots & [\hat{\mathbf{K}}_{pq}]^{ij}_{1r} \\
[\hat{\mathbf{K}}_{pq}]^{ij}_{21} & [\hat{\mathbf{K}}_{pq}]^{ij}_{22} & \cdots & [\hat{\mathbf{K}}_{pq}]^{ij}_{2r} \\
\vdots & \vdots & \ddots & \vdots \\
[\hat{\mathbf{K}}_{pq}]^{ij}_{r1} & [\hat{\mathbf{K}}_{pq}]^{ij}_{r2} & \cdots & [\hat{\mathbf{K}}_{pq}]^{ij}_{rr}
\end{bmatrix},\quad
[{}^{LS}\hat{\mathbf{K}}]^{ij}=\begin{bmatrix}
{}^{LS}\hat{\mathbf{K}}^{ij}_{11} & {}^{LS}\hat{\mathbf{K}}^{ij}_{12} & \cdots & {}^{LS}\hat{\mathbf{K}}^{ij}_{1r} \\
{}^{LS}\hat{\mathbf{K}}^{ij}_{21} & {}^{LS}\hat{\mathbf{K}}^{ij}_{22} & \cdots & {}^{LS}\hat{\mathbf{K}}^{ij}_{2r} \\
\vdots & \vdots & \ddots & \vdots \\
{}^{LS}\hat{\mathbf{K}}^{ij}_{r1} & {}^{LS}\hat{\mathbf{K}}^{ij}_{r2} & \cdots & {}^{LS}\hat{\mathbf{K}}^{ij}_{rr}
\end{bmatrix},$$

and in which $p, q = 1, 2, r$ is the largest term of Fourier series used in the analysis, ${}^{LS}\hat{\mathbf{K}}^{ij}_{mn}$ is a 2×2 matrix given in Eq. (A.6) in Appendix A, and

$$[\hat{\mathbf{K}}_{11}]^{ij}_{mn} = \begin{bmatrix} \hat{K}^{ij}_{1,mn} & \hat{K}^{ij}_{2,mn} \\ \hat{K}^{ij}_{2,mn} & \hat{K}^{ij}_{5,mn} \end{bmatrix}, \quad [\hat{\mathbf{K}}_{22}]^{ij}_{mn} = \begin{bmatrix} \hat{K}^{ij}_{1,mn} & -\hat{K}^{ij}_{2,mn} \\ -\hat{K}^{ij}_{2,mn} & \hat{K}^{ij}_{6,mn} \end{bmatrix},$$

$$[\hat{\mathbf{K}}_{12}]^{ij}_{mn} = ([\hat{\mathbf{K}}_{21}]^{ij}_{mn})^{\mathrm{T}} = \begin{bmatrix} \hat{K}^{ij}_{3,mn} & \hat{K}^{ij}_{4,mn} \\ -\hat{K}^{ij}_{4,mn} & \hat{K}^{ij}_{5,mn} \end{bmatrix},$$

in which $\hat{K}^{ij}_{l,mn}, l = 1, 2, \ldots, 6$ are given in Eq. (A.4). The overall mass matrix for the whole plate $\hat{\mathbf{M}}$ in Eq. (1), the elements of which are given in Eqs. (A.5) and (A.7), can be assembled in exactly the same way as the overall stiffness matrix $\hat{\mathbf{K}}$. It is noted that both matrices $\hat{\mathbf{K}}$ and $\hat{\mathbf{M}}$ are symmetric. The non-dimensional displacement vector of plate $\hat{\mathbf{u}}$ is given by

$$\hat{\mathbf{u}} = \{\hat{\mathbf{u}}^{11}, \hat{\mathbf{u}}^{12}, \ldots, \hat{\mathbf{u}}^{1N}; \hat{\mathbf{u}}^{21}, \hat{\mathbf{u}}^{22}, \ldots, \hat{\mathbf{u}}^{2N}; \hat{\mathbf{u}}^{31}\}^{\mathrm{T}},$$

$$\hat{\mathbf{u}}^{ij} = \{\hat{\mathbf{u}}^{ij}_1, \hat{\mathbf{u}}^{ij}_2, \ldots, \hat{\mathbf{u}}^{ij}_r\}^{\mathrm{T}}, \quad \hat{\mathbf{u}}^{ij}_m = \{\hat{\omega}^{ij}_m, \hat{\theta}^{ij}_m\}^{\mathrm{T}},$$

where $\hat{\omega}^{ij}_m$ and $\hat{\theta}^{ij}_m$ are given in Eq. (A.3). Boundary conditions at edges $x = 0$ and $x = L$ can be introduced after or prior to the assembly of $\hat{\mathbf{K}}$, $\hat{\mathbf{M}}$ and $\hat{\mathbf{u}}$, while boundary conditions at edges $y = 0$ and $y = b$ have already been considered in the elements of matrices $\hat{\mathbf{K}}$, $\hat{\mathbf{M}}$.

The above assembly of matrices is illustrated for a 4-panel plate with only two orthogonal stiffeners. The stiffness and mass matrices can be assembled in a similar way for a plate with more than two orthogonal stiffeners, say, a 9-panel plate with two orthogonal stiffeners in each direction.

It is noteworthy that the treatment of the longitudinal stiffener in this paper is somewhat different from that in Ref. [10]. In the current approach the longitudinal stiffener is considered separately from the plate and the contribution of the longitudinal stiffener to the structural behavior of the whole plate is considered in $[\hat{\mathbf{K}}_{\mathrm{c}}]$ and $[\hat{\mathbf{M}}_{\mathrm{c}}]$, while in Ref. [10] the longitudinal stiffener is considered in Eqs. (A.4) and (A.5) in a similar way as for the transverse stiffener. The current approach requires that one of the nodal lines of the finite strip division of the plate be placed on the longitudinal stiffener, while in Ref. [10] there is no such restriction and the longitudinal stiffener can be placed between two nodal lines. However, it is expected that the current approach is more accurate since the deflection of the longitudinal stiffener is exactly the same as only one nodal line that goes through the stiffener, while in Ref. [10] the deflection of the longitudinal stiffener depends on two nodal lines. Moreover, the position of the longitudinal stiffener is easier and clearer to locate in the current approach. In Ref. [10] the position of the longitudinal stiffener would jump from strip to strip when misplacement of the stiffener is introduced. Since the position of the stiffener is important in the localization analysis, the current approach has some advantages over that of Ref. [10].

The eigenvalue problem (1) can be solved by standard techniques. The mth eigenvalue μ_m corresponds to the natural frequency of the mth vibration mode of the plate. Knowing the eigenvalue μ_m and the associated eigenvector $\hat{\mathbf{u}}_m$, the corresponding vibration mode of the plate $F_m(x, y)$ can then be determined from Eq. (A.1).

2.2. Numerical results

The variation of the free vibration mode shapes with small misplacements of the two intermediate stiffeners is of interest. Assume that the misplacements of the intermediate stiffeners are d_x and d_y in the x and y directions, respectively, such that $L_1 = L/2 + d_x$, $L_2 = L/2 - d_x$, $b_1 = b/2 + d_y$, and $b_2 = b/2 - d_y$. The non-dimensional misplacements can be denoted by $\delta_x = d_x/b$ and $\delta_y = d_y/b$.

For simplifying the presentation, if the two stiffeners are identical, their parameter subscripts TS, LS, x, and y will be replaced by S or dropped, e.g., ω_S for the flexural rigidity, τ_S for the torsional rigidity, δ_S for the misplacement of the stiffeners, $\hat{m}_w$ for the mass, and $\hat{m}_\theta$ for the mass moment of inertia. The subscript S has double meanings, *Stiffener* and *Same* in two directions.

To verify the natural frequencies and mode shapes of the free vibration of a four-panel plate, with different values of misplacements of the intermediate stiffeners, obtained using the compound strip method presented in this section, the results are compared with those obtained using a finite element method, STARDYNE. It is observed that the numerical results of both methods agree very well, even for much higher modes. Hence, the formulations using compound strip method are suitable for the study of vibration mode localization of the four-panel stiffened plate.

2.2.1. Vibration mode localization

In Fig. 3, the first mode of a plate with four edges clamped, $L/b = 1/1$, $\omega_S = 20$, $\tau_S = 0.1$, $\hat{m}_w = 0.1$, and $\hat{m}_\theta = 0.0$ are plotted in (a) for $\delta_x = \delta_y = 0$ and in (b) for $\delta_x = 0.01$, $\delta_y = -0.05$. When the plate is perfectly periodic, i.e., $\delta_x = \delta_y = 0$, the vibration mode is symmetric about the stiffeners; the amplitudes of vibration in all four panels are the same. When the intermediate stiffeners are misplaced slightly, the localization in the vibration mode can be clearly seen—vibration is mostly confined to one panel.

The vibration mode localization may be characterized by the ratios $\rho_{11,kl}$ of the maximum deflections of the centers of the four panels, i.e.,

$$\rho_{11,22} = \frac{|z^{(11)}|_{\max}}{|z^{(22)}|_{\max}}, \quad \rho_{11,12} = \frac{|z^{(11)}|_{\max}}{|z^{(12)}|_{\max}}, \quad \rho_{11,21} = \frac{|z^{(11)}|_{\max}}{|z^{(21)}|_{\max}}. \tag{2}$$

If $\rho_{11,kl}$ is close to 1, the maximum deflections in the two panels compared are comparable; whereas when $\rho_{11,kl} \ll 1$ or $\rho_{11,kl} \gg 1$, the maximum deflections in the two panels compared are significantly different and deformation is confined, i.e., the vibration mode is localized.

The value of the non-dimensional quantity $\hat{m}_\theta$, which is related to the mass moment of inertia of stiffeners, is usually very small (less than the order of 10^{-4}). It is observed that, in a realistic range, $\hat{m}_\theta$ has little effect on $\rho_{11,kl}$. Hence, $\hat{m}_\theta = 0$ is taken in the remainder of this paper unless specified.

The vibration mode localization indicators $\rho_{11,kl}$ of a four-panel square plate are plotted in Figs. 4–11 as functions of the major parameters of the stiffeners, i.e., the flexural rigidity ω_S, the torsional rigidity τ_S, the mass $\hat{m}_w$, and the misplacements δ_x and δ_y. Some selected mode shapes are also presented in each figure to illustrate the turns and jumps of $\rho_{11,kl}$. When the stiffened square plate is symmetric about $x = y$, $\rho_{11,12}$ is the same as $\rho_{11,21}$. When the flexural rigidity of the stiffeners ω_S is very large, the stiffened plate can be considered as simply supported at the stiffeners.

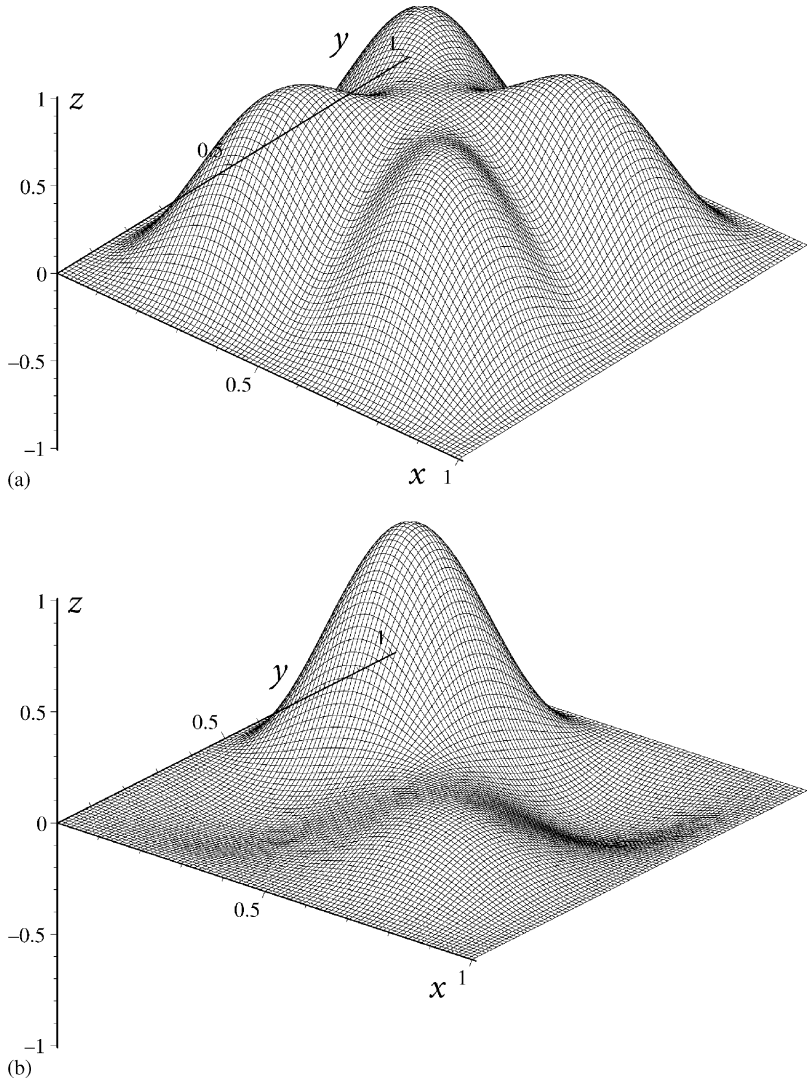

Fig. 3. The first vibration mode for a four-panel square plate with $\omega_S = 20$, $\tau_S = 0.1$, $\hat{m}_w = 0.1$, $\hat{m}_\theta = 0.0$. (a) $\delta_x = \delta_y = 0.0$; (b) $\delta_x = 0.01$ and $\delta_y = -0.05$.

$\rho_{11,kl}$ versus ω_S and $\hat{m}_w$: Ratio $\rho_{11,22}$ of the first and the second vibration modes of a four-panel square plate with $\delta_S = 0.01$ and $\tau_S = 0.1$ are plotted versus ω_S from 0 to 100 and $\hat{m}_w$ from 0 to 1 in Figs. 4 and 5, respectively.

It is seen in Fig. 4 that the mass of the stiffener $\hat{m}_w$ has little effect on ratio $\rho_{11,22}$ of the first mode when $\omega_S < 10$ or $\omega_S > 50$, i.e., $\rho_{11,22}$ do not change much with the change of ω_S in these ranges. When ω_S is large, the small effect of $\hat{m}_w$ is expected since the mass of the stiffener has no effect at all on the vibration behavior of the plate if the plate is simply supported at the stiffener.

However, the flexural rigidity ω_S of the stiffeners has dramatic effects on $\rho_{11,22}$, especially for the higher modes as seen in Fig. 5. When $\omega_S \to 0$, the mode shapes are similar to those of a

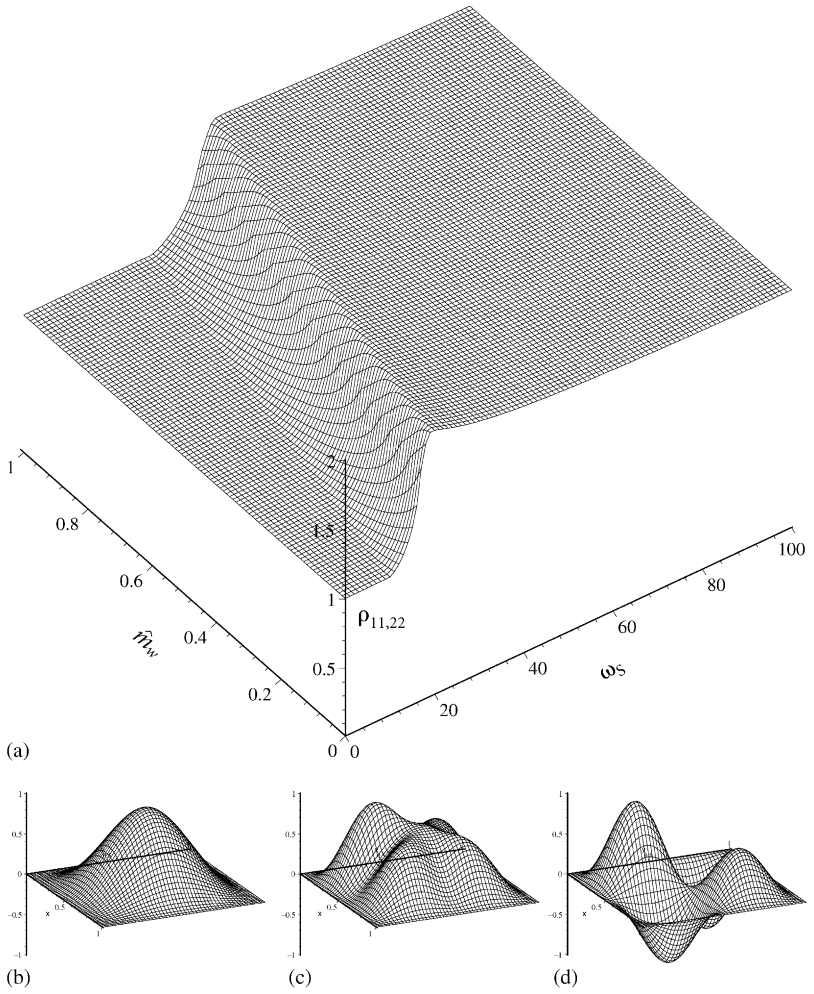

Fig. 4. $\rho_{11,22}$ of the first mode of a four-panel square plate with $\delta_S = 0.01$ and $\tau_S = 0.1$. (a) $\rho_{11,22}$ versus ω_S and $\hat{m}_w$; (b) mode shape, $\hat{m}_w = 1$, $\omega_S = 0$, $\rho_{11,22} = 1.00$; (c) mode shape, $\hat{m}_w = 1$, $\omega_S = 37$, $\rho_{11,22} = 1.28$; (d) mode shape, $\hat{m}_w = 1$, $\omega_S = 50$, $\rho_{11,22} = 1.774$.

one-panel plate. When $\omega_S \to \infty$, the mode shapes are similar to those of a four-panel plate with intermediate simple supports.

The minimum value of the flexural rigidity ω_S to make the plate be considered as simply supported at the stiffener depends on different vibration modes. For instance, as seen in Fig. 4 that when $\omega_S = 50$ the first vibration modes are very similar to that of a four-panel plate with two intermediate simple supports, and $\hat{m}_w$ has little effect on the mode shapes in the range from 0 to 1. However, as shown in Fig. 5, $\omega_S = 64$ is still not large enough for the second mode of the plate to be considered as simply supported at the stiffeners.

$\rho_{11,kl}$ versus ω_S and τ_S: Ratios $\rho_{11,kl}$ of the first vibration mode of a four-panel square plate with $\delta_S = 0.01$ and $\hat{m}_w = 0.1$ are plotted versus ω_S from 0 to 100 and torsional rigidity τ_S from 0 to 1 in Fig. 6 for $\rho_{11,22}$ and in Fig. 7 for $\rho_{11,12}$, respectively.

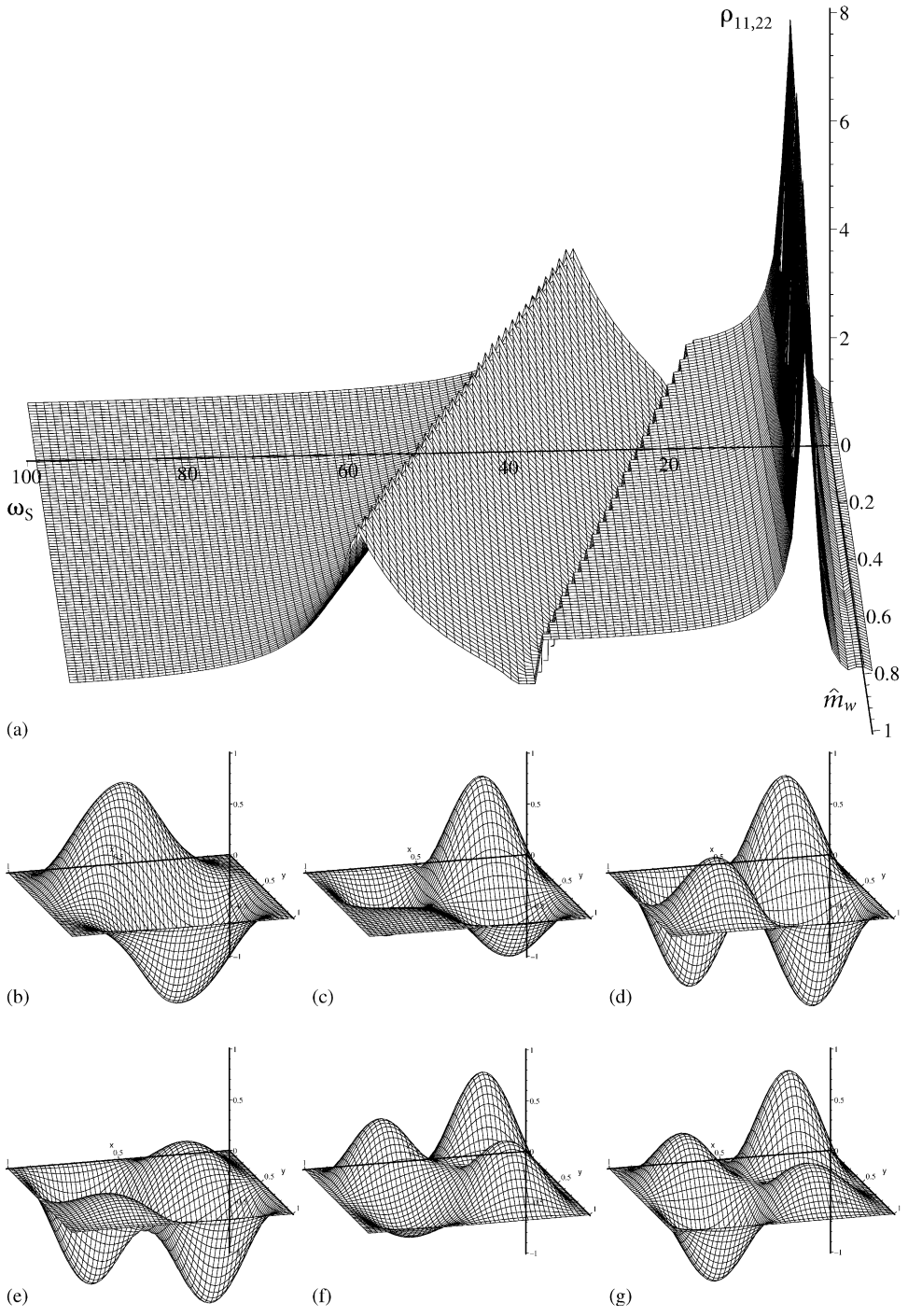

Fig. 5. $\rho_{11,22}$ of the second mode of a four-panel square plate with $\delta_S = 0.01$ and $\tau_S = 0.1$. (a) $\rho_{11,22}$ versus ω_S and $\hat{m}_w$; (b) mode shape, $\hat{m}_w = 1$, $\omega_S = 0$, $\rho_{11,22} = 1.12$; (c) mode shape, $\hat{m}_w = 1$, $\omega_S = 8$, $\rho_{11,22} = 8.41$; (d) mode shape, $\hat{m}_w = 1$, $\omega_S = 40$, $\rho_{11,22} = 1.81$; (e) mode shape, $\hat{m}_w = 1$, $\omega_S = 42$, $\rho_{11,22} = 1.00$; (f) mode shape, $\hat{m}_w = 1$, $\omega_S = 64$, $\rho_{11,22} = 3.87$; (g) mode shape, $\hat{m}_w = 1$, $\omega_S = 80$, $\rho_{11,22} = 1.45$.

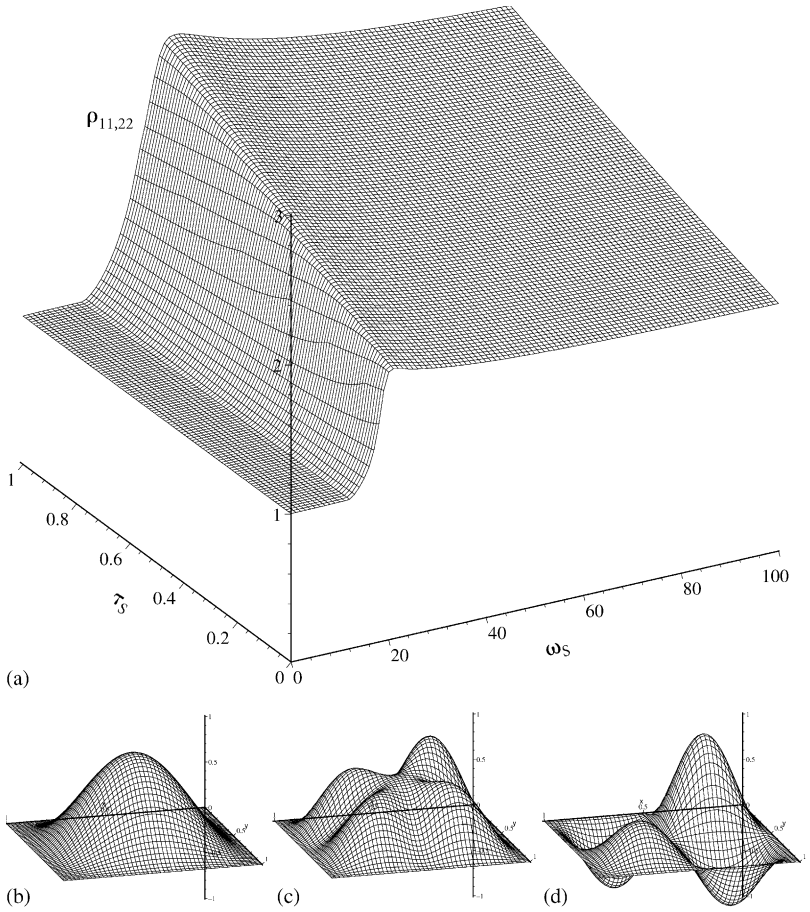

Fig. 6. $\rho_{11,22}$ of the first mode of a four-panel square plate with $\delta_S = 0.01$ and $\hat{m}_w = 0.1$. (a) $\rho_{11,22}$ versus ω_S and τ_S; (b) mode shape, $\tau_S = 1$, $\omega_S = 0$, $\rho_{11,22} = 1.00$; (c) mode shape, $\tau_S = 1$, $\omega_S = 20$, $\rho_{11,22} = 1.41$; (d) mode shape, $\tau_S = 1$, $\omega_S = 50$, $\rho_{11,22} = 2.49$.

As shown in Fig. 6, for $\omega_S < 10$, both the flexural rigidity ω_S and the torsional rigidity τ_S have little effect on $\rho_{11,22}$. For $10 < \omega_S < 50$, both of ω_S and τ_S have dramatic effect on $\rho_{11,22}$, especially when $10 < \omega_S < 20$, a small increase of ω_S would result in a large increase of $\rho_{11,22}$. When $\omega_S > 50$, the larger the torsional rigidity τ_S, the larger the ratio $\rho_{11,22}$, while the change of ω_S does not affect $\rho_{11,22}$ much.

In Fig. 7, for $\omega_S < 10$, both the flexural rigidity ω_S and the torsional rigidity τ_S have little effect on $\rho_{11,12}$, this is similar to that in Fig. 6 for $\rho_{11,22}$, which indicates that the first mode shape of the four-panel plate changes little with the change of both ω_S and τ_S in the range of $\tau_S < 1$. For $10 < \omega_S < 50$, both ω_S and τ_S have dramatic effect on $\rho_{11,12}$, especially when $\omega_S \approx 28$, a small change of ω_S and τ_S would lead to a large change of $\rho_{11,12}$. When $\omega_S > 50$, ratio $\rho_{11,12}$ increases slightly with the increase of τ_S, while the change of ω_S does not affect $\rho_{11,12}$ much.

$\rho_{11,kl}$ versus ω_S and δ_S: Figs. 8 and 9 show the ratios $\rho_{11,kl}$ versus ω_S from 0 to 100 and δ_S from 0 to 0.05 for the first vibration mode of a four-panel square plate with $\tau_S = 0.1$ and $\hat{m}_w = 0.1$. It is

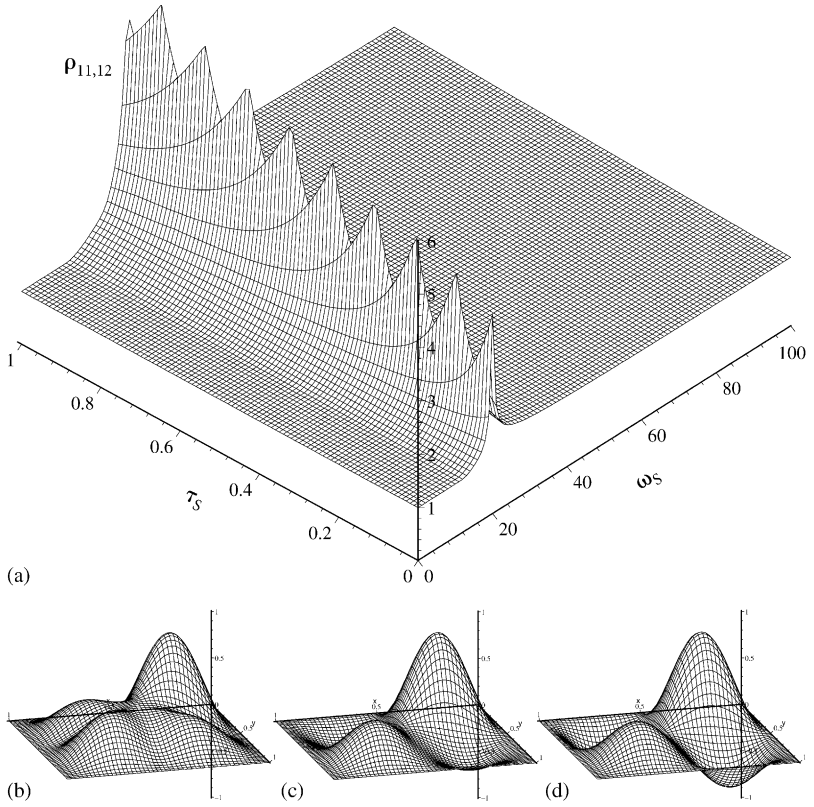

Fig. 7. $\rho_{11,12}$ of the first mode of a four-panel square plate with $\delta_S = 0.01$ and $\hat{m}_w = 0.1$. (a) $\rho_{11,12}$ versus ω_S and τ_S; (b) mode shape, $\omega_S = 27$, $\tau_S = 0.80$, $\rho_{11,12} = 5.14$; (c) mode shape, $\omega_S = 28$, $\tau_S = 0.91$, $\rho_{11,12} = 5.51$; (d) mode shape, $\omega_S = 30$, $\tau_S = 0.91$, $\rho_{11,12} = 2.63$.

observed that when $\delta_S = 0$, i.e., when the plate is perfectly periodic, $\rho_{11,kl} = 1$ for all ω_S. This is expected—since, when there is no misplacement of the stiffeners, the plate is symmetric about the stiffeners, the vibration mode deflections of the four panels have the same value and there is no vibration mode localization. It is also observed that except for very small values of ω_S, the misplacement of the stiffeners δ_S has a dramatic effect on the vibration mode localization of the four-panel plate. The larger the misplacement δ_S, the more significant the vibration mode localization.

It is also seen in Figs. 8 and 9 that when $10 < \omega_S < 50$, the effect of ω_S on the vibration localization is most significant, especially for larger value of misplacement δ_S. On the other hand, the change of the flexural rigidity ω_S has little effect on the first vibration mode localization when $\omega_S > 50$.

$\rho_{11,kl}$ versus δ_x and δ_y: The vibration mode indicator $\rho_{11,22}$ of the first mode is presented in Fig. 10 in terms of misplacement δ_x and δ_y from 0 to 0.05 for a four-panel square plate with $\omega_S = 20$, $\tau_S = 0.1$, and $\hat{m}_w = 0.1$. It is observed that even a very small misplacement change may significantly affect the vibration behavior of the plate, e.g., as seen in Fig. 10, when $\delta_y = 0$, ratio $\rho_{11,22}$ jumps from 1.59 for $\delta_x = 0.035$ to 3.54 for $\delta_x = 0.05$. By comparing the vibration

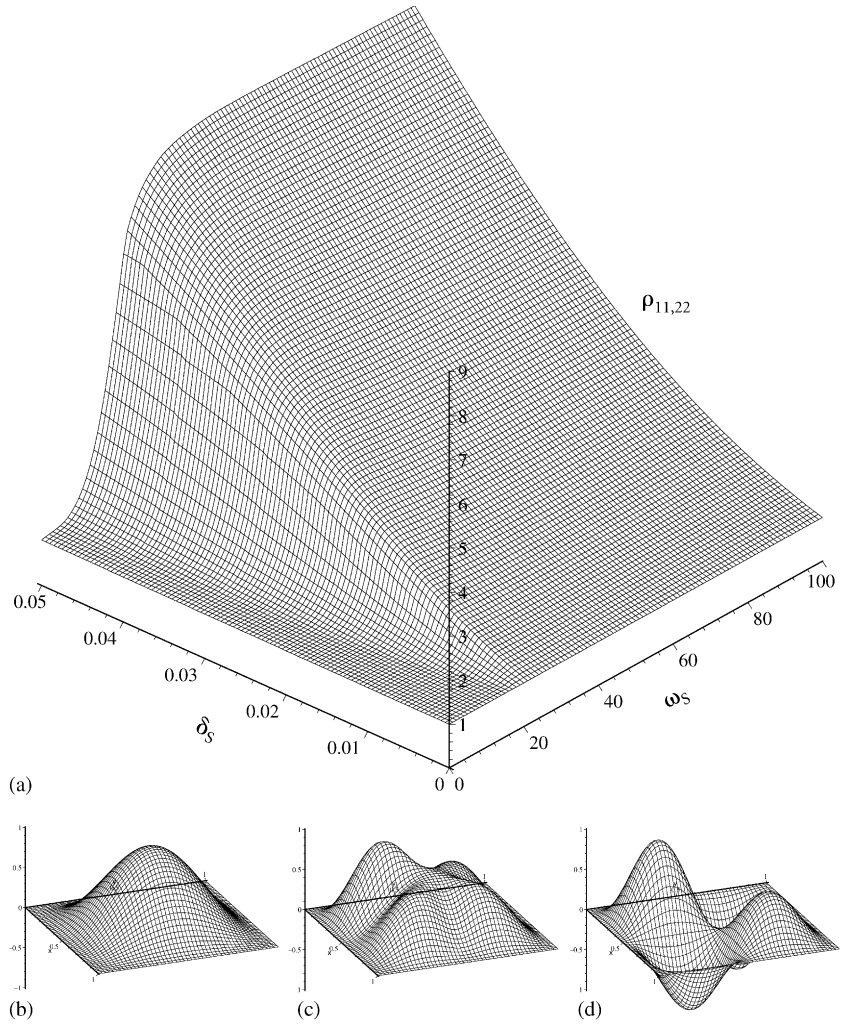

Fig. 8. $\rho_{11,22}$ of the first mode of a four-panel square plate with $\tau_S = 0.1$ and $\hat{m}_w = 0.1$. (a) $\rho_{11,22}$ versus ω_S and δ_S; (b) mode shape, $\delta_S = 0.01$, $\omega_S = 0$, $\rho_{11,22} = 1.00$; (c) mode shape, $\delta_S = 0.01$, $\omega_S = 18$, $\rho_{11,22} = 1.39$; (d) mode shape, $\delta_S = 0.01$, $\omega_S = 50$, $\rho_{11,22} = 1.77$.

modes around the jumps of $\rho_{11,22}$, it is observed that the jumps of $\rho_{11,22}$ are due to the significant change in the mode shapes.

$\rho_{11,kl}$ versus τ_S and $\hat{m}_w$: To compare the effects of the torsional rigidity and the mass of the stiffeners on the vibration mode localization behavior of the four-panel plate, $\rho_{11,22}$ of the first mode is plotted in Fig. 11 versus τ_S and $\hat{m}_w$ from 0 to 1 for a square plate with $\omega_S = 20$ and $\delta_S = 0.05$. It is seen that in term of vibration mode localization, the mass $\hat{m}_w$ of the stiffeners has more significant effect than the torsional rigidity τ_S when the flexural rigidity ω_S is not large. However, when ω_S is so large that the plate can be considered simply supported at the stiffeners, $\hat{m}_w$ has no effect on the vibration behavior of the plate, while the change of τ_S would affect the structural behavior of the whole plate.

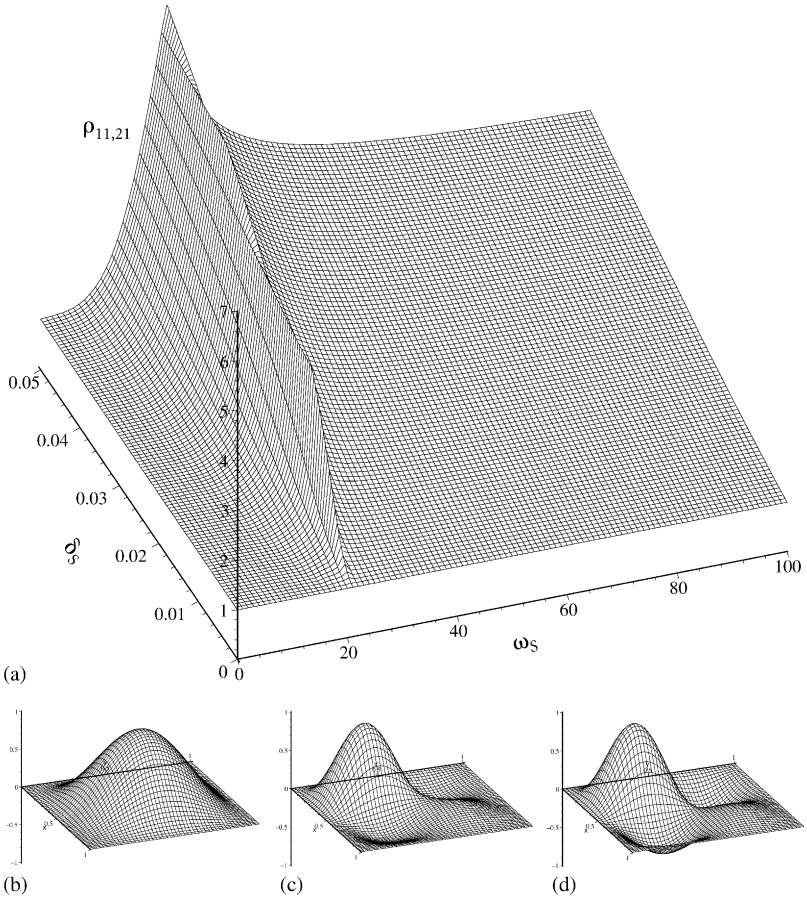

Fig. 9. $\rho_{11,21}$ of the first mode of a four-panel square plate with $\tau_S = 0.1$ and $\hat{m}_w = 0.1$. (a) $\rho_{11,21}$ versus ω_S and δ_S; (b) mode shape, $\delta_S = 0.05$, $\omega_S = 0$, $\rho_{11,21} = 1.02$; (c) mode shape, $\delta_S = 0.05$, $\omega_S = 23$, $\rho_{11,21} = 6.85$; (d) mode shape, $\delta_S = 0.05$, $\omega_S = 100$, $\rho_{11,21} = 3.06$.

Summary: From the study of Figs. 3–11, it is observed that the misplacement δ_S and the flexural rigidity ω_S of the stiffeners have a much more significant effect on vibration mode localization than the torsional rigidity τ_S and the mass $\hat{m}_w$ in realistic ranges. Hence, it is reasonable to focus on the effects of ω_S and δ_S in the vibration localization study.

3. Forced vibration localization using Galerkin's method

In Section 2, the vibration mode localization of a uniform four-panel plate with four edges clamped and two intermediate stiffeners as shown in Fig. 1 was studied using the compound strip method. In this section, the forced vibration localization is investigated using Galerkin's method based on the mode shapes obtained by the compound strip method in the previous section.

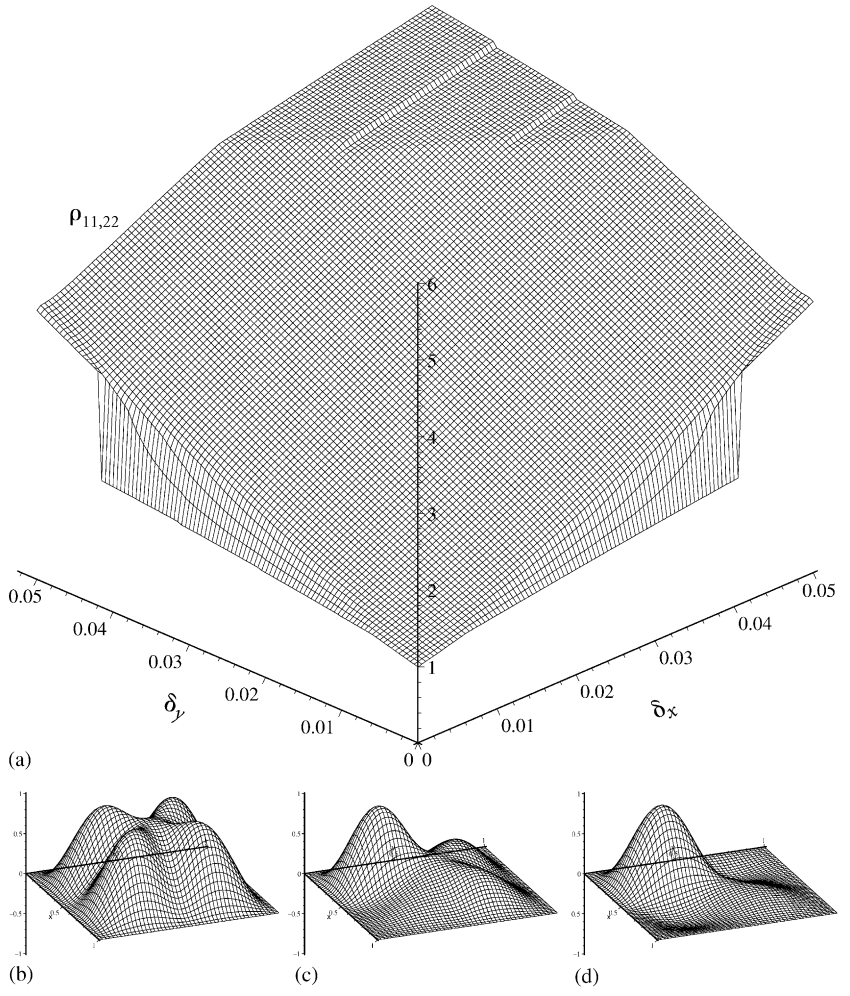

Fig. 10. $\rho_{11,22}$ of the first mode of a four-panel square plate with $\omega_S = 20$, $\tau_S = 0.1$ and $\hat{m}_w = 0.1$. (a) $\rho_{11,22}$ versus δ_x and δ_y; (b) mode shape, $\delta_x = 0.0005$, $\delta_y = 0.0005$, $\rho_{11,22} = 1.03$; (c) mode shape, $\delta_x = 0.035$, $\delta_y = 0.0005$, $\rho_{11,22} = 2.20$; (d) mode shape, $\delta_x = 0.05$, $\delta_y = 0.05$, $\rho_{11,22} = 5.27$.

Suppose that the plate is subjected to a harmonic concentrated load $P_0 \sin \Omega t$ applied at the center of Panel 11, i.e., point $(L_1/2, b_1/2)$ as shown in Fig. 1, in which P_0 is a given constant with the dimension of force and Ω is the circular frequency of excitation. For the thin elastic, isotropic plate, the flexural deflection $z(x, y, t)$ during vibration is governed by a linear partial differential equation

$$D\left(\frac{\partial^4 z}{\partial x^4} + 2\frac{\partial^4 z}{\partial x^2 \partial y^2} + \frac{\partial^4 z}{\partial y^4}\right) + \rho h \frac{\partial^2 z}{\partial t^2} = P_0 \sin \Omega t \delta\left(x - \frac{L_1}{2}\right)\delta\left(y - \frac{b_1}{2}\right), \tag{3}$$

where δ is the Dirac delta function.

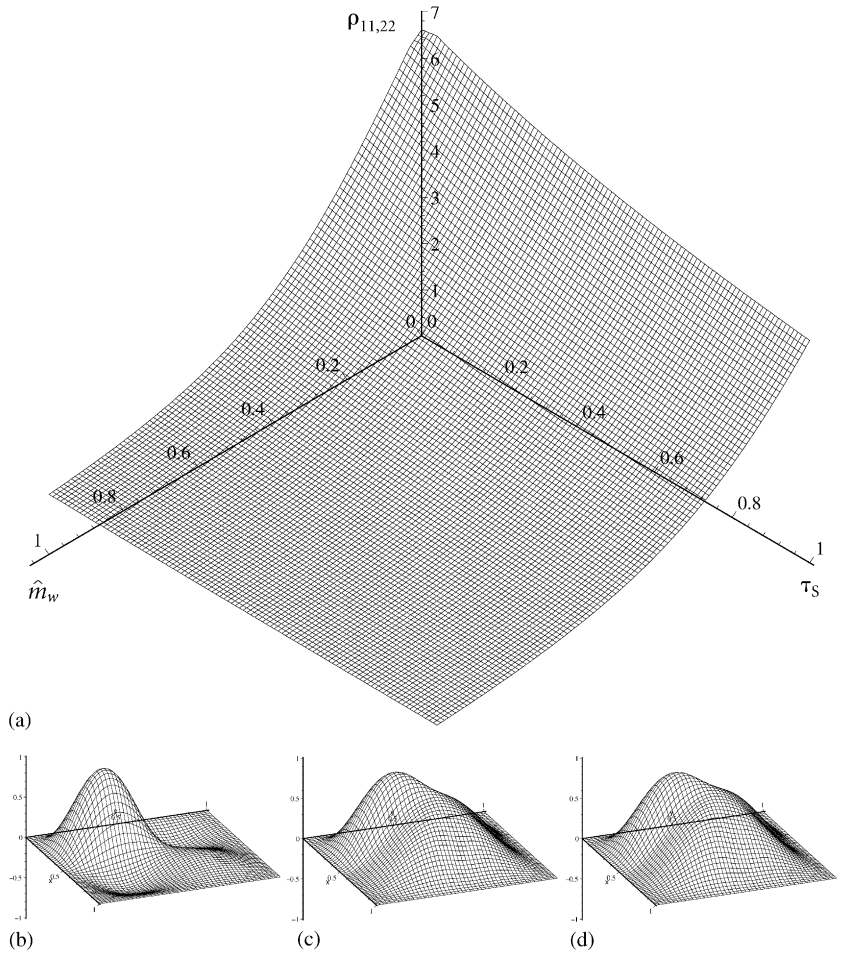

Fig. 11. $\rho_{11,22}$ of the first mode of a four-panel square plate with $\delta_S = 0.05$ and $\omega_S = 20$. (a) $\rho_{11,22}$ versus τ_S and $\hat{m}_w$; (b) mode shape, $\tau_S = 0$, $\hat{m}_w = 0$, $\rho_{11,22} = 6.61$; (c) mode shape, $\tau_S = 0$, $\hat{m}_w = 1$, $\rho_{11,22} = 1.31$; (d) mode shape, $\tau_S = 1$, $\hat{m}_w = 1$, $\rho_{11,22} = 1.23$.

The transverse deflection $z(x, y, t)$ is assumed to be of the form

$$z(x, y, t) = z_c(x, y, t) + z_p(x, y, t), \tag{4}$$

in which $z_c(x, y, t)$ is the complementary solutions, which satisfies the homogeneous equation (3) with $P_0 = 0$, and $z_p(x, y, t)$ is a particular solution of Eq. (3). By using Galerkin's method, approximate expressions of z_c and z_p for the plate, which is in the undeformed state at $t = 0$, can be written as

$$z_c(x, y, t) = \sum_{m=1}^{K} q_m^c F_m(x, y) \sin \omega_m t, \tag{5}$$

and

$$z_p(x,y,t) = \sum_{m=1}^{K} q_m(t) F_m(x,y), \tag{6}$$

in which ω_m is the mth circular natural frequency of the plate, $F_m(x,y)$ is the associated mth vibration mode obtained in Section 2, K is an integer chosen so as to achieve a satisfactory accuracy, q_m^c are constants to be determined by the initial conditions $z|_{t=0} = 0$, $\partial z/\partial t|_{t=0} = 0$, $q_m(t)$ are functions of time t.

Substituting the particular solution (6) into the equation of motion (7), multiplying both sides by $F_n(x,y)$, $n = 1,2,\ldots,K$, and integrating with respect to x from 0 to L and with respect to y from 0 to b results in a system of coupled ordinary differential equations

$$\rho h \mathbf{A}\ddot{\mathbf{q}}(t) + D\mathbf{B}\mathbf{q}(t) = \mathbf{f}\sin \Omega t, \tag{7}$$

where

$$\mathbf{q}(t) = \{q_1(t), q_2(t), \ldots, q_K(t)\}^{\mathrm{T}}, \quad \mathbf{f} = P_0\{F_1(x_0,y_0), F_2(x_0,y_0), \ldots, F_K(x_0,y_0)\}^{\mathrm{T}},$$

and the elements of the $K \times K$ matrices $\mathbf{A}$ and $\mathbf{B}$ are given by

$$a_{mn} = \int_{x=0}^{L}\int_{y=0}^{b} F_m(x,y)F_n(x,y)\,\mathrm{d}x\,\mathrm{d}y,$$

$$b_{mn} = \int_{x=0}^{L}\int_{y=0}^{b} [\nabla^4 F_m(x,y)]F_n(x,y)\,\mathrm{d}x\,\mathrm{d}y, \tag{8}$$

where $\nabla^4 = \partial^4/\partial x^4 + 2\partial^4/\partial x^2\partial y^2 + \partial^4/\partial y^4$.

As stated before, the free vibration mode $F_m(x,y)\sin\omega_m t$ satisfies the homogeneous equation (3) with $P_0 = 0$, i.e.,

$$D[\nabla^4 F_m(x,y)\sin\omega_m t] + \rho h \frac{\partial^2}{\partial t^2}[F_m(x,y)\sin\omega_m t] = 0,$$

or

$$\nabla^4 F_m(x,y) = \frac{\rho h \omega_m^2}{D} F_m(x,y). \tag{9}$$

Substituting Eq. (9) into b_{mn} in Eq. (8) results in $b_{mn} = \rho h \omega_m^2 a_{mn}/D$. Therefore, Eq. (7) can be rewritten as

$$\mathbf{A}\ddot{\mathbf{q}}(t) + \mathbf{A}\mathbf{W}\mathbf{q}(t) = \frac{\sin \Omega t}{\rho h}\mathbf{f}, \tag{10}$$

in which $\mathbf{W} = \mathrm{diag}\{\omega_1^2, \omega_2^2, \ldots, \omega_K^2\}$. Multiplying both sides of Eq. (10) by $\mathbf{A}^{-1}$ leads to a series of decoupled ordinary differential equations

$$\ddot{q}_m(t) + \omega_m^2 q_m(t) = p_m \sin \Omega t, \tag{11}$$

where p_m is the mth element of vector $\mathbf{A}^{-1}\mathbf{f}/\rho h$.

Non-resonant case $\Omega \neq \omega_m$: When $\Omega \neq \omega_m$, the general solution to Eq. (11) is

$$q_m(t) = q_m(0)\cos\omega_m t + \frac{\dot{q}_m(0)}{\omega_m}\sin\omega_m t + \frac{p_m}{\omega_m^2 - \Omega^2}\sin\Omega t. \tag{12}$$

If the plate is at rest when $t = 0$, i.e., $q_m(0) = \dot{q}_m(0) = 0$, Eq. (12) becomes

$$q_m(t) = d_m \sin \Omega t, \quad d_m = \frac{p_m}{\omega_m^2 - \Omega^2}. \tag{13}$$

Substituting the flexural deflection (4) into the initial condition $\partial z/\partial t|_{t=0} = 0$ leads to

$$q_m^c = -d_m \frac{\Omega}{\omega_m}. \tag{14}$$

The transverse displacement of the plate can then be written as

$$z(x, y, t) = \sum_{m=1}^{K} q_m^c F_m(x, y) \sin \omega_m t + \sin \Omega t \sum_{m=1}^{K} d_m F_m(x, y). \tag{15}$$

To non-dimensionalize the formulation, two reference quantities are introduced. One is the constant concentrated load P_h, which, when applied at the center, makes the center transverse deflection equal to h for a one-panel simply supported rectangular plate with length L, width b, and uniform thickness h. P_h is equal to $Dh/(\alpha' b^2)$, where α' is a constant related to the ratio of L and b and is given by Eq. (147) in Ref. [11]. The other quantity is the first natural frequency of this one-panel simply supported plate given by

$$\omega_0 = \frac{\pi^2(L^2 + b^2)}{L^2 b^2}\sqrt{\frac{D}{\rho h}}.$$

Employing the following non-dimensional quantities:

$$\hat{P}_0 = \frac{P_0}{P_h}, \quad \hat{\Omega} = \frac{\Omega}{\omega_0}, \quad \hat{\omega}_m = \omega_m \cdot \frac{b^2}{\pi^2}\sqrt{\frac{\rho h}{D}}, \quad \hat{\nu}_m = \frac{\omega_m}{\omega_0} = \hat{\omega}_m\left(1 + \frac{b^2}{L^2}\right)^{-1},$$
$$\hat{p}_m = \frac{\pi^2 p_m}{b\omega_0^2}, \quad \tau = t \cdot \frac{\pi^2}{b^2}\sqrt{\frac{D}{\rho h}}, \quad \hat{d}_m = \frac{\pi^2}{b} d_m, \quad \xi = \frac{x}{b}, \quad \eta = \frac{y}{b}, \quad \hat{z} = \frac{\pi^2}{b} z, \tag{16}$$

Eq. (15) can be written in a non-dimensional form as

$$\hat{z}(\xi, \eta, \tau) = \sum_{m=1}^{K}\left[\left(1 + \frac{b^2}{L^2}\right)\frac{\hat{\Omega}}{\hat{\omega}_m} \cdot \frac{\hat{p}_m}{\hat{\Omega}^2 - \hat{\nu}_m^2} \hat{F}_m(\xi, \eta) \sin \hat{\omega}_m \tau\right]$$
$$+ \sin\left[\left(1 + \frac{b^2}{L^2}\right)\hat{\Omega}\tau\right] \sum_{m=1}^{K} \frac{\hat{p}_m}{\hat{\nu}_m^2 - \hat{\Omega}^2} \hat{F}_m(\xi, \eta), \tag{17}$$

where $\hat{F}_m(\xi, \eta)$ is the non-dimensional form of the mth vibration mode $F_m(x, y)$. It is noteworthy that this research deals with plates without damping. If damping is considered, the first part of Eq. (17), which depends on the initial conditions, will eventually vanish.

When $\Omega \neq \omega_m$, i.e., when $\hat{\Omega} \neq \hat{\nu}_n$, the forced vibration response $\hat{z}$ is finite as can be seen in Eq. (17).

Resonant case $\Omega = \omega_n$: When $\Omega = \omega_n$ or $\hat{\Omega} = \hat{\nu}_n$, the four-panel plate is in resonance in mode n. For $m \neq n$, the solution of Eq. (11) is given by Eq. (12). For $m = n$, the solution of Eq. (11) is

$$q_n(t) = q_n(0) \cos \omega_n t + \frac{\dot{q}_n(0)}{\omega_n} \sin \omega_n t - \frac{p_n}{2\omega_n} t \cos \Omega t. \tag{18}$$

Employing the initial conditions and the non-dimensional quantities in Eq. (16), the non-dimensional transverse displacement of the plate is given by

$$\hat{z}(\xi,\eta,\tau)=\sum_{\substack{m=1\\ m\neq n}}^{K}\left\{\left(1+\frac{b^2}{L^2}\right)\frac{\hat{\Omega}}{\hat{\omega}_m}\sin\hat{\omega}_m\tau-\sin\left[\left(1+\frac{b^2}{L^2}\right)\hat{\Omega}\tau\right]\right\}\frac{\hat{p}_m}{\hat{\Omega}^2-\hat{v}_m^2}\hat{F}_m(\xi,\eta)$$
$$+\frac{\hat{p}_n}{2\hat{v}_n^2}\hat{F}_n(\xi,\eta)\left\{\sin\hat{\omega}_n\tau-\tau\cdot\hat{\omega}_n\cos\left[\left(1+\frac{b^2}{L^2}\right)\hat{\Omega}\tau\right]\right\}. \tag{19}$$

It can be seen in the last term of Eq. (19) that the deflection $\hat{z}(\xi,\eta,\tau)$ increases linearly with time τ. Since the plate is in resonance in mode n, the forced vibration response $\hat{z}(\xi,\eta,\tau)$ is dominated by the nth mode when the time τ is large, which implies that the response is in the shape of mode n. Hence, the forced vibration localization is the same as the mode localization of mode n.

3.1. Numerical results

Numerical results of the response of a plate subjected to a harmonic concentrated load $P_0\sin\Omega t$ at the center of Panel 11 obtained by Galerkin's method presented in this section are compared with those obtained by a finite element method using STARDYNE. It is observed that the dynamic responses obtained by these two methods agree very well. When plotted, the difference is hardly visible except for near some of the peak deflections. The excellent agreement indicates that Galerkin's method is suitable for the analysis of forced vibration of the four-panel plates.

3.1.1. Forced vibration localization

The variation of the forced vibration response with a small misplacement of the intermediate stiffeners is of interest. Similar to the analysis of vibration mode localization, the localization phenomena in forced vibration of the four-panel plate shown in Fig. 1 may be characterized by ratios $\hat{\rho}_{11,kl}$ of the maximum deflections of the centers of the four panels in a given time period, i.e.,

$$\hat{\rho}_{11,22}=\frac{|\hat{z}^{(11)}|_{\max}}{|\hat{z}^{(22)}|_{\max}},\quad \hat{\rho}_{11,12}=\frac{|\hat{z}^{(11)}|_{\max}}{|\hat{z}^{(12)}|_{\max}},\quad \hat{\rho}_{11,21}=\frac{|\hat{z}^{(11)}|_{\max}}{|\hat{z}^{(21)}|_{\max}},$$

where $|\hat{z}^{(kl)}|_{\max}$, $k,l=1,2$, is the non-dimensional maximum deflection at the center of panel kl in a specified period of time. If $\hat{\rho}_{11,kl}$ is close to 1, the maximum deflections in the two panels compared are comparable; whereas when $\hat{\rho}_{11,kl}\ll 1$ or $\hat{\rho}_{11,kl}\gg 1$, the maximum deflections in the two panels compared are significantly different and deformation is confined or the vibration is localized.

The value of excitation force $\hat{P}_0$ does not affect the relative amplitude ratios $\hat{\rho}_{11,kl}$ owing to the linearity of the system. Therefore, $\hat{P}_0=-0.01$ is used in the analysis of forced vibration localization in the remaining of this paper.

Special attention must be paid when selecting the period of time used to find $|\hat{z}^{(kl)}|_{\max}$. To illustrate, in Fig. 12, the non-dimensional deflection $\hat{z}^{(11)}$ of the center of Panel 11 is plotted versus the non-dimensional time τ for a four-panel square plate clamped at four edges with $\omega_S=20$, $\tau_S=0.1$, $\hat{m}_w=0.1$, $\delta_x=0.025$, $\delta_y=0.05$, and various excitation frequencies $\hat{\Omega}$. The first two non-dimensional natural frequencies of the four-panel plate are $\hat{v}_1=5.06$ and $\hat{v}_2=5.50$.

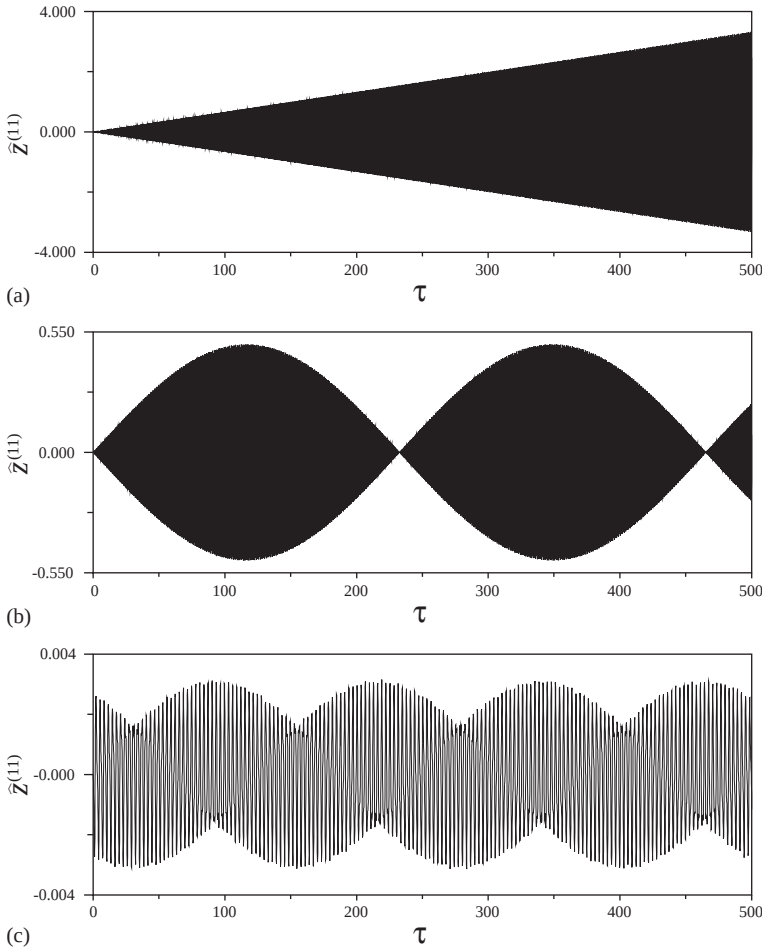

Fig. 12. Forced vibration response of a four-panel square plate with $\omega_S = 20$, $\tau_S = 0.1$, $\hat{m}_w = 0.1$, $\delta_x = 0.025$, $\delta_y = 0.05$. (a) $\hat{\Omega} = \hat{\nu}_1 = 5.06$; (b) $\hat{\Omega} = 5.05$; (c) $\hat{\Omega} = 2.50$.

As observed in Fig. 12, when $\hat{\Omega} = \hat{\nu}_1$, i.e., when the plate is in resonance in the first mode, the deflection amplitudes of the forced vibration increase linearly with the increase of time. When the excitation frequency is very close to one of the natural frequencies, i.e., when $\hat{\Omega} = 5.05$, the forced vibration response is *amplitude modulated*. It is observed that $|\hat{z}^{(11)}|_{\max}$ occurs at a much larger value of τ for $\hat{\Omega} = 5.05$ than that for the non-resonant case when $\hat{\Omega} = 2.5$. Hence, a much longer period of time must be taken to find $|\hat{z}^{(11)}|_{\max}$ when the plate is approaching the situation of resonance. For the non-resonant cases, the non-dimensional time period τ in Eq. (16) is chosen as from 0 to 500 in the remaining of this paper unless specified.

Ratio $\hat{\rho}_{11,22}$ of a four-panel square plate with $\omega_S = 20$, $\tau_S = 0.1$, and $\hat{m}_w = 0.1$ are plotted as functions of the non-dimensional misplacements δ_x and δ_y ranging from -0.05 to 0.05 in Fig. 13(a) for $\hat{\Omega} = 5.0$ and in (b) for $\hat{\Omega} = 5.5$. The first non-dimensional natural frequency for perfect stiffener position $\delta_S = 0.0$ is 5.49. The roughness and the jumps and turns of the ratios $\hat{\rho}_{11,22}$ are due to the superposition of the various modes.

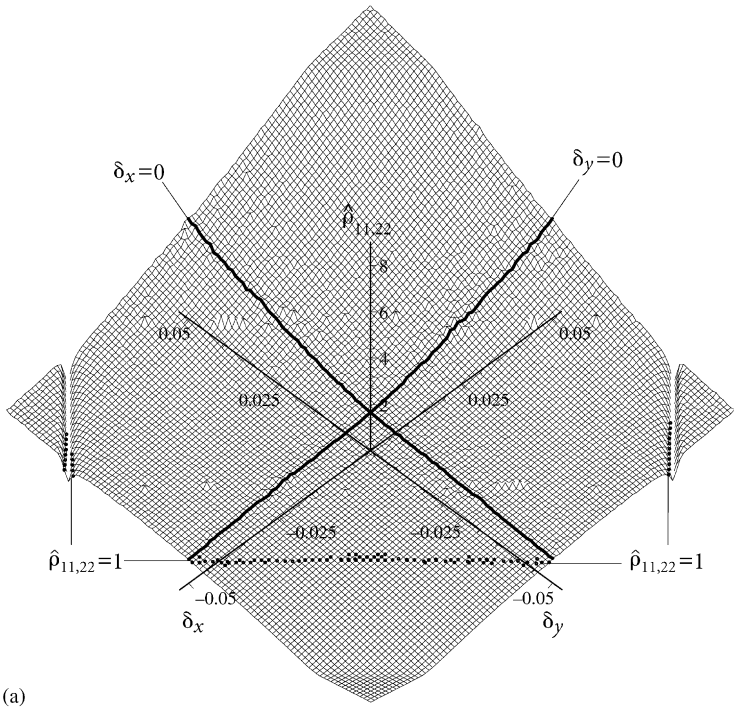

(a)

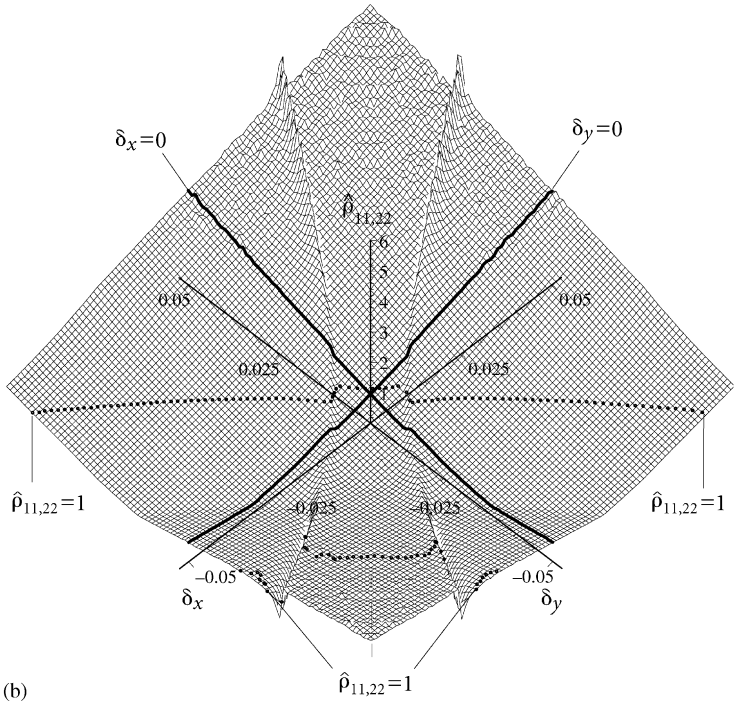

(b)

Fig. 13. $\hat{\rho}_{11,22}$ of a four-panel square plate with $\omega_S = 20$, $\tau_S = 0.1$, $\hat{m}_w = 0.1$. (a) $\hat{\Omega} = 5.0$; (b) $\hat{\Omega} = 5.5$.

It is seen in Fig. 13 that, when $\delta_x > 0$, $\delta_y > 0$, and except in the vicinity of those jumps, ratio $\hat{\rho}_{11,22}$ increases with the increase of the misplacements of the two intermediate stiffeners; in other words, the larger the misplacements, the more significant the forced vibration localization. When $\delta_x = \delta_y = 0.0$ and the excitation frequency is close to the first natural frequency 5.49, as seen in Fig. 13(b), the ratio $\hat{\rho}_{11,22}$ is very close to 1, which means that Panel 22 has the same magnitude of response as Panel 11 where the dynamic load is applied.

3.1.2. Vibration reduction

By deliberately introducing disorder in the intermediate rib-stiffeners into the plate, the magnitudes of vibration of some of the four panels may be reduced.

Ratios $\hat{\rho}_{11,22}$ and $\hat{\rho}_{11,21} = \hat{\rho}_{11,12}$ of plates with $L/b = 1/1$, $\omega_S = 50$, $\tau_S = 0.1$, and $\hat{m}_w = 0.1$ are plotted as a function of $\hat{\Omega}$ from 0.5 to 7.0 in Fig. 14 for $\delta_S = 0.0$ and 0.03, respectively. Ratio $\hat{\rho}_{11,12}$ is the same as $\hat{\rho}_{11,21}$ because of the symmetry of the plate about $x = y$. The first five non-dimensional natural frequencies of the stiffened plates are given in Table 1.

It is noteworthy that the deflection at the exciting point $z^{(11)}$ is not necessarily the maximum deflection of the whole plate. Whether or not the maximum deflection at the exciting point $|\hat{z}^{(11)}|_{\max}$ is the maximum deflection of the entire plate depends on the value of the exiting frequency $\hat{\Omega}$ and the combination of the misplacements δ_x and δ_y. It can be observed in Fig. 14 that $|\hat{z}^{(21)}|_{\max} = |\hat{z}^{(12)}|_{\max}$ gives the maximum deflection of the centers of the four plate panels when $\hat{\Omega} = 6.0$ and $\delta_S = 0.03$, since $\hat{\rho}_{11,21} = \hat{\rho}_{11,12}$ is smaller than 1 while $\hat{\rho}_{11,22}$ is larger than 1. When $\hat{\Omega} = 5.75$ and $\delta_S = 0.0$, the ratios $\hat{\rho}_{11,kl}$ are all smaller than 1, which indicates that, among the maximum deflections of the centers of the four plate panels, the maximum deflection at the exciting point $|\hat{z}^{(11)}|_{\max}$ is the smallest instead of the largest. On the other hand, when $\hat{\Omega} < 5$, i.e., when the exciting frequency is smaller than the first natural frequency of the stiffened plate, $\hat{\rho}_{11,kl} \gg 1$, i.e., $|\hat{z}^{(11)}|_{\max}$ is much greater than the other three maximum deflections, which means vibration is strongly localized in Panel 11.

When $\delta_S = 0.0$ and $\hat{\Omega}$ approaching the natural frequencies shown in Table 1, ratios $\hat{\rho}_{11,kl}$ are all close to 1, which indicates that the deflection responses at the centers of the four panels have the same magnitude, i.e., vibration is not localized. The reason is that, for a perfect plate, all of the vibration modes are symmetric about the stiffeners and the deflections of all panels of the plate are the same. When the excitation frequency $\hat{\Omega}$ approaches one of the natural frequencies, only the corresponding vibration mode is dominant in the forced vibration response of the plate, and when the plate is in resonance, forced vibration localization is the same as mode localization.

For vibration reduction in Panels 21 and 12, as can be observed in Fig. 14(b); when the excitation frequency $1.2 < \hat{\Omega} < 5.9$, $\hat{\rho}_{11,21} = \hat{\rho}_{11,12}$ of $\delta_S = 0.03$ is larger than that of $\delta_S = 0.0$, one has better vibration reduction. However, when $\hat{\Omega} < 1.2$, there is no significant vibration improvement in Panels 21 and 12 by changing the positions of the stiffeners from their perfect positions to $\delta_S = 0.03$. When $5.9 < \hat{\Omega} < 6.35$, $\hat{\rho}_{11,21} = \hat{\rho}_{11,12}$ of $\delta_S = 0.03$ is less than 1, meaning that the magnitudes of the vibration response in Panels 21 and 12 are larger than that in Panel 11.

On the other hand, as can be seen in Fig. 14(a), when $\delta_S = 0.03$, ratio $\hat{\rho}_{11,22}$ is always larger than 1, which indicates that the forced vibration response is always localized for all values of $\hat{\Omega}$ shown. Furthermore, for all values of $\hat{\Omega}$ shown, ratio $\hat{\rho}_{11,22}$ of $\delta_S = 0.03$ is always larger than that of

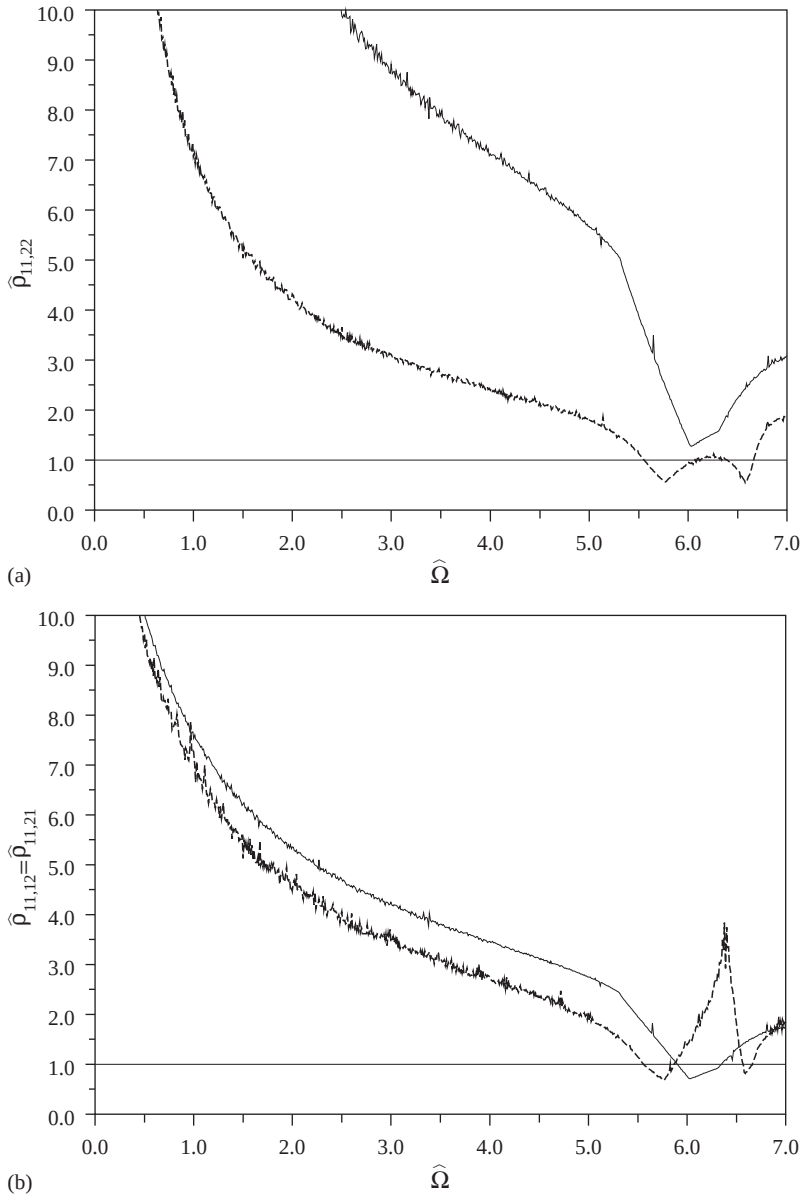

Fig. 14. Vibration reduction of a four-panel square plate with $\omega_S = 50$, $\tau_S = 0.1$, and $\hat{m}_w = 0.1$; ------, $\delta_S = 0.0$; ——, $\delta_S = 0.03$. (a) $\hat{\rho}_{11,22}$; (b) $\hat{\rho}_{11,12} = \hat{\rho}_{11,21}$.

Table 1
Frequency comparison

	$\hat{\nu}_1$	$\hat{\nu}_2$	$\hat{\nu}_3$	$\hat{\nu}_4$	$\hat{\nu}_5$
$\delta_S = 0.00$	5.558	6.393	6.394	6.664	10.731
$\delta_S = 0.03$	5.319	6.313	6.464	7.174	10.473

$\delta_S = 0.0$, especially when the excitation frequency $\hat{\Omega} < 5$, which implies that by purposely misplacing the stiffeners the forced vibration response in Panel 22 can be reduced.

One may hope that, by introducing another combination of the misplacements δ_x and δ_y, all the three ratios $\hat{\rho}_{11,12}$, $\hat{\rho}_{11,21}$, and $\hat{\rho}_{11,22}$ would be greater than 1 for larger $\hat{\Omega}$ value, or in other words, the vibration would be mainly localized in Panel 11 for all $\hat{\Omega}$. However, it has been found that this is unfortunately impossible for a four-panel plate with only two intermediate rib-stiffeners. The forced vibration localization is expected to be more significant for larger plates with more panels and more misplaced rib-stiffeners, which will be the focus of future research.

4. Conclusions

In this paper, the compound strip method and Galerkin's method are applied to analyze vibration localization of four-panel rectangular plates with two intermediate stiffeners in two orthogonal directions. It is found that this approach works well on both the free vibration and forced vibration of plates. Although only the results of the case when all four edges clamped and only two stiffeners are presented, the method has also been successfully applied to study the plates with other boundary conditions and more stiffeners.

In the study of vibration mode localization, it is observed that a small disorder of the rib-stiffeners may significantly affect the vibration mode localization of the whole plate. The mass of the stiffeners has a more significant effect on mode localization than the torsional rigidity when the flexural rigidity of the stiffeners is not large. However, when the flexural rigidity of the stiffeners is so large that the plate can be considered as simply supported at the stiffeners, the mass of the stiffeners has no effect on the vibration behavior of the plate, while the change of the torsional rigidity would affect the structural behavior of the whole plate. On the other hand, it is observed that the misplacement and the flexural rigidity of the stiffeners have a much more significant effect on vibration mode localization than the torsional rigidity and the mass in realistic ranges. Except for very small values of flexural rigidity of the stiffeners, the larger the misplacement of the stiffeners, the more significant the vibration mode localization of the plate.

In forced vibration localization, when the plate is in resonance, only the resonant mode is dominant in the forced vibration response, and the forced vibration localization is the same as the mode localization of the resonant mode. It is found that the deflection at the point of excitation is not necessarily the maximum deflection of the plate. It is also observed that, at some values of the excitation frequency, the larger the misplacement of the stiffeners, the more significant the forced vibration localization.

The theory of vibration localization is applicable to vibration reduction, the essence of which is that a small disorder in the periodicity of structures will lead to a significant change in the mode shapes and localization in the vibration responses. By deliberately introducing irregularity into the stiffeners, the vibration of some of the panels of the plate may be reduced. Although it is desired to reduce the vibration of all panels for all frequencies, this is not feasible for a plate with only two rib-stiffeners. The forced vibration localization is expected to be more significant for larger plates with more rib-stiffeners, which will be the subject of future research. A very important application is to study localization of vibration propagation in large building floor systems so that design guidelines can be formulated to reduce annoying vibrations floor systems due to human activities.

Acknowledgements

The research for this paper was supported, in part, by the Natural Sciences and Engineering Research Council of Canada through Grant No. OGPO131355. The authors are grateful to the referees for the constructive comments which helped to improve the paper.

Appendix A. Stiffness and mass matrices of compound strip method

The first paper on the finite strip method was presented by Cheung [12] on plate-bending problems using a simply supported rectangular strip. The finite strip method has been proven to be more efficient than the finite element method for certain problems, e.g., the analysis of plate type structures. Puckett and Gutkowski [9] developed the compound strip method by extending the finite strip method for the analysis of plates with transverse and longitudinal stiffeners or column supports. The stiffness of the stiffeners and columns is accounted for by the direct stiffness method.

In this appendix, the non-dimensional stiffness and mass matrices of a compound strip and an individual stiffener are presented.

A.1. Stiffness and mass matrices of compound strip $\hat{\mathbf{K}}^{ij}_{mn}$ *and* $\hat{\mathbf{M}}^{ij}_{mn}$

Consider a typical jth uniform strip of ith span of width l_{ij}, length b, and thickness h with an intermediate transverse stiffener as shown in Fig. 15. The edges $y = 0$ and $y = b$ can be simply supported or clamped. In this study, the in-plane displacements are neglected. The superscript "ij" indicates the jth strip of the ith span of a rectangular plate.

From the studies of Cheung [13], the out-of-plane displacement function is given by

$$z^{ij}(x,y,t) = \sum_{m=1}^{\infty} F_m^{ij}(x,y)\mathrm{e}^{\mathrm{i}\omega t}$$
$$= \sum_{m=1}^{\infty} [C_1^{ij} w_m^{ij} + C_2^{ij}\theta_m^{ij} + C_3^{ij} w_m^{i(j+1)} + C_4^{ij}\theta_m^{i(j+1)}] Y_m(y)\mathrm{e}^{\mathrm{i}\omega t}, \tag{A.1}$$

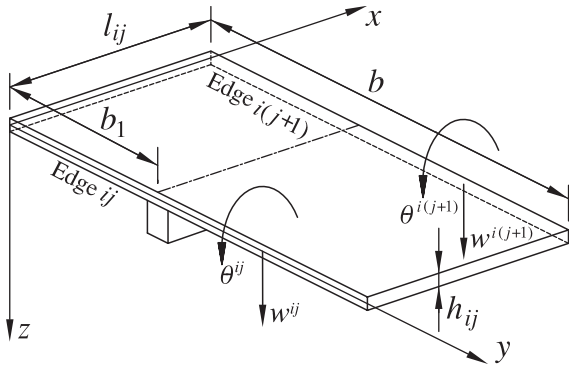

Fig. 15. A typical ijth finite strip with a transverse stiffener.

where ω is the natural frequency, w_m^{ij}, $w_m^{i(j+1)}$, θ_m^{ij}, and $\theta_m^{i(j+1)}$ are the displacement parameters (mth term of the Fourier series) of edges j and $j+1$, $Y_m(y)$ is the boundary function, and

$$C_1^{ij} = 1 - \frac{3x^2}{l_{ij}^2} + \frac{2x^3}{l_{ij}^3}, \quad C_2^{ij} = x - \frac{2x^2}{l_{ij}} + \frac{x^3}{l_{ij}^2}, \quad C_3^{ij} = \frac{3x^2}{l_{ij}^2} - \frac{2x^3}{l_{ij}^3}, \quad C_4^{ij} = \frac{x^3}{l_{ij}^2} - \frac{x^2}{l_{ij}}.$$

According to Ref. [10], the total strain energy and kinetic energy of the compound strip shown in Fig. 15 are $U^{ij} = {}^{P}U^{ij} + {}^{TS}U^{ij}$, and $T^{ij} = {}^{P}T^{ij} + {}^{TS}T^{ij}$, respectively, where the scripts "P" and "TS" denote "Plate" and "Transverse Stiffener". The stiffness and mass matrices of the compound strip are therefore given by

$$\mathbf{K}_{mn}^{ij} = {}^{P}\mathbf{K}_{mn}^{ij} + {}^{TS}\mathbf{K}_{w,mn}^{ij} + {}^{TS}\mathbf{K}_{\theta,mn}^{ij}, \quad \mathbf{M}_{mn}^{ij} = {}^{P}\mathbf{M}_{mn}^{ij} + {}^{TS}\mathbf{M}_{w,mn}^{ij} + {}^{TS}\mathbf{M}_{\theta,mn}^{ij}, \tag{A.2}$$

in which the stiffness and mass matrices of the plate strip ${}^{P}\mathbf{K}_{mn}^{ij}$ and ${}^{P}\mathbf{M}_{mn}^{ij}$ can be found in Ref. [13], the stiffness and mass matrices of the transverse stiffener in bending ${}^{TS}\mathbf{K}_{w,mn}^{ij}$, ${}^{TS}\mathbf{M}_{w,mn}^{ij}$ and in torsion ${}^{TS}\mathbf{K}_{\theta,mn}^{ij}$, ${}^{TS}\mathbf{M}_{\theta,mn}^{ij}$ can be found in Refs. [9] and [10].

The non-dimensionalized dynamic equilibrium equations of the compound plate strip shown in Fig. 15 are

$$(\hat{\mathbf{K}}_{mn}^{ij} - \mu\hat{\mathbf{M}}_{mn}^{ij})\hat{\boldsymbol{\delta}}_m^{ij} = \mathbf{0}, \tag{A.3}$$

where $\hat{\boldsymbol{\delta}}_m^{ij} = \{\hat{w}_m^{ij}, \hat{\theta}_m^{ij}, \hat{w}_m^{i(j+1)}, \hat{\theta}_m^{i(j+1)}\}^{\mathrm{T}}$, $\hat{w}_{mn}^{ij} = w_m^{ij}/b$, $\hat{\theta}_m^{ij} = \theta_m^{ij}$, $\mu = b^4\rho h\omega^2/(\pi^4 D)$ is the non-dimensional frequency, $D = Eh^3/[12(1-\nu^2)]$, ρ and h are the mass density and thickness of the plate, ν is the Poisson ratio, E is Young's modulus, $\hat{\mathbf{K}}_{mn}^{ij}$ is the non-dimensional stiffness matrix for the ijth compound plate strip given by

$$\hat{\mathbf{K}}_{mn}^{ij} = \begin{bmatrix} \hat{K}_{1,mn}^{ij} & \hat{K}_{2,mn}^{ij} & \hat{K}_{3,mn}^{ij} & \hat{K}_{4,mn}^{ij} \\ \hat{K}_{2,mn}^{ij} & \hat{K}_{5,mn}^{ij} & -\hat{K}_{4,mn}^{ij} & \hat{K}_{6,mn}^{ij} \\ \hat{K}_{3,mn}^{ij} & -\hat{K}_{4,mn}^{ij} & \hat{K}_{1,mn}^{ij} & -\hat{K}_{2,mn}^{ij} \\ \hat{K}_{4,mn}^{ij} & \hat{K}_{6,mn}^{ij} & -\hat{K}_{2,mn}^{ij} & \hat{K}_{5,mn}^{ij} \end{bmatrix}, \tag{A.4}$$

where

$$\begin{aligned}
\hat{K}_{1,mn}^{ij} &= {}^{P}\hat{K}_{1,mn}^{ij} + 12\hat{k}_{w,mn}^{ij}\omega_{TS}^{j} + 36\hat{k}_{\theta,mn}^{ij}\tau_{TS}^{j}, \\
\hat{K}_{2,mn}^{ij} &= {}^{P}\hat{K}_{2,mn}^{ij} + 6\hat{l}_{ij}\hat{k}_{w,mn}^{ij}\omega_{TS}^{j} + 3\hat{l}_{ij}\hat{k}_{\theta,mn}^{ij}\tau_{TS}^{j}, \\
\hat{K}_{3,mn}^{ij} &= {}^{P}\hat{K}_{3,mn}^{ij} - 12\hat{k}_{w,mn}^{ij}\omega_{TS}^{j} - 36\hat{k}_{\theta,mn}^{ij}\tau_{TS}^{j}, \\
\hat{K}_{4,mn}^{ij} &= {}^{P}\hat{K}_{4,mn}^{ij} + 6\hat{l}_{ij}\hat{k}_{w,mn}^{ij}\omega_{TS}^{j} + 3\hat{l}_{ij}\hat{k}_{\theta,mn}^{ij}\tau_{TS}^{j}, \\
\hat{K}_{5,mn}^{ij} &= {}^{P}\hat{K}_{5,mn}^{ij} + 4\hat{l}_{ij}^2\hat{k}_{w,mn}^{ij}\omega_{TS}^{j} + 4\hat{l}_{ij}^2\hat{k}_{\theta,mn}^{ij}\tau_{TS}^{j}, \\
\hat{K}_{6,mn}^{ij} &= {}^{P}\hat{K}_{6,mn}^{ij} + 2\hat{l}_{ij}^2\hat{k}_{w,mn}^{ij}\omega_{TS}^{j} - \hat{l}_{ij}^2\hat{k}_{\theta,mn}^{ij}\tau_{TS}^{j},
\end{aligned}$$

in which $\hat{l}_{ij} = l_{ij}/b$, and

$$
\begin{aligned}
{}^{P}\hat{K}^{ij}_{1,mn} &= \tfrac{13}{35}\hat{l}_{ij}\eta_{2,mn} + \frac{12}{5\hat{l}_{ij}}\eta_{1,mn} + \frac{12}{\hat{l}^3_{ij}}\eta_{0,mn},\\
{}^{P}\hat{K}^{ij}_{2,mn} &= \tfrac{11}{210}\hat{l}^2_{ij}\eta_{2,mn} + \left(v + \tfrac{1}{5}\right)\eta_{1,mn} + \frac{6}{\hat{l}^2_{ij}}\eta_{0,mn},\\
{}^{P}\hat{K}^{ij}_{3,mn} &= \tfrac{9}{70}\hat{l}_{ij}\eta_{2,mn} - \frac{12}{5\hat{l}_{ij}}\eta_{1,mn} - \frac{12}{\hat{l}^3_{ij}}\eta_{0,mn},\\
{}^{P}\hat{K}^{ij}_{4,mn} &= -\tfrac{13}{420}\hat{l}^2_{ij}\eta_{2,mn} + \tfrac{1}{5}\eta_{1,mn} + \frac{6}{\hat{l}^2_{ij}}\eta_{0,mn},\\
{}^{P}\hat{K}^{ij}_{5,mn} &= \tfrac{1}{105}\hat{l}^3_{ij}\eta_{2,mn} + \tfrac{4}{15}\hat{l}_{ij}\eta_{1,mn} + \frac{4}{\hat{l}_{ij}}\eta_{0,mn},\\
{}^{P}\hat{K}^{ij}_{6,mn} &= -\tfrac{1}{140}\hat{l}^3_{ij}\eta_{2,mn} - \tfrac{1}{15}\hat{l}_{ij}\eta_{1,mn} + \frac{2}{\hat{l}_{ij}}\eta_{0,mn},
\end{aligned}
$$

and

$$
\eta_{0,mn} = \frac{1}{b}\int_0^b Y_m(y)\,Y_n(y)\,\mathrm{d}y, \quad \eta_{1,mn} = b\int_0^b Y'_m(y)\,Y'_n(y)\,\mathrm{d}y,
$$

$$
\eta_{2,mn} = b^3\int_0^b Y''_m(y)\,Y''_n(y)\,\mathrm{d}y,
$$

$$
\hat{k}^{ij}_{w,mn} = \frac{Y_m(b_1)\,Y_n(b_1)b^3}{\pi l^3_{ij}}, \quad \hat{k}^{ij}_{\theta,mn} = \frac{Y'_m(b_1)\,Y'_n(b_1)b^3}{30\pi l_{ij}},
$$

$$
\omega^{j}_{TS} = \frac{\pi(EI)^{j}_{TS}}{bD}, \quad \tau^{j}_{TS} = \frac{\pi(GJ)^{j}_{TS}}{bD}.
$$

The non-dimensional mass matrix of the compound strip

$$
\hat{\mathbf{M}}^{ij}_{mn} = \begin{bmatrix}
\hat{M}^{ij}_{1,mn} & \hat{M}^{ij}_{2,mn} & \hat{M}^{ij}_{3,mn} & \hat{M}^{ij}_{4,mn}\\
\hat{M}^{ij}_{2,mn} & \hat{M}^{ij}_{5,mn} & -\hat{M}^{ij}_{4,mn} & \hat{M}^{ij}_{6,mn}\\
\hat{M}^{ij}_{3,mn} & -\hat{M}^{ij}_{4,mn} & \hat{M}^{ij}_{1,mn} & -\hat{M}^{ij}_{2,mn}\\
\hat{M}^{ij}_{4,mn} & \hat{M}^{ij}_{6,mn} & -\hat{M}^{ij}_{2,mn} & \hat{M}^{ij}_{5,mn}
\end{bmatrix}, \tag{A.5}
$$

where

$$
\begin{aligned}
\hat{M}^{ij}_{1,mn} &= \tilde{m}^{P}\hat{M}^{ij}_{1,mn} + 36\hat{m}^{ij}_{\theta,mn}, \quad \hat{M}^{ij}_{2,mn} = \tilde{m}^{P}\hat{M}^{ij}_{2,mn} + 3\hat{l}_{ij}\hat{m}^{ij}_{\theta,mn},\\
\hat{M}^{ij}_{3,mn} &= \tilde{m}^{P}\hat{M}^{ij}_{3,mn} - 36\hat{m}^{ij}_{\theta,mn}, \quad \hat{M}^{ij}_{4,mn} = \tilde{m}^{P}\hat{M}^{ij}_{4,mn} + 3\hat{l}_{ij}\hat{m}^{ij}_{\theta,mn},\\
\hat{M}^{ij}_{5,mn} &= \tilde{m}^{P}\hat{M}^{ij}_{5,mn} + 4\hat{l}^2_{ij}\hat{m}^{ij}_{\theta,mn}, \quad \hat{M}^{ij}_{6,mn} = \tilde{m}^{P}\hat{M}^{ij}_{6,mn} - 4\hat{l}^2_{ij}\hat{m}^{ij}_{\theta,mn},
\end{aligned}
$$

in which

$$
{}^{P}\hat{M}^{ij}_{1,mn} = \frac{13\hat{l}_{ij}}{35}, \quad {}^{P}\hat{M}^{ij}_{2,mn} = \frac{11\hat{l}_{ij}}{210}, \quad {}^{P}\hat{M}^{ij}_{3,mn} = \frac{9\hat{l}_{ij}}{70},
$$

$$
{}^{P}\hat{M}^{ij}_{4,mn} = -\frac{13\hat{l}^{2}_{ij}}{420}, \quad {}^{P}\hat{M}^{ij}_{5,mn} = \frac{\hat{l}^{3}_{ij}}{105}, \quad {}^{P}\hat{M}^{ij}_{6,mn} = -\frac{3\hat{l}^{3}_{ij}}{420}
$$

$$
\hat{m}^{ij}_{w,TS} = \pi^4 \frac{(\rho A)^{j}_{TS}}{\rho h b}, \quad \hat{m}^{ij}_{\theta,TS} = \pi^4 \frac{(\rho J)^{j}_{TS}}{\rho h b^3} \quad \tilde{m} = \pi^4 \eta_{0,mn} + \hat{m}^{ij}_{w,mn}.
$$

A.2. Stiffness and mass matrices ${}^{LS}\hat{\mathbf{K}}^{ij}_{mn}$ and ${}^{LS}\hat{\mathbf{M}}^{ij}_{mn}$

To derive the stiffness and mass matrices of a longitudinal stiffener, consider a stiffener of flexural rigidity $(EI)^{ij}_{LS}$ and torsional rigidity $(GJ)^{ij}_{LS}$ placed along the jth nodal line of the ith span. The scripts "LS" stands for "Longitudinal Stiffener".

The stiffener may be considered as a beam element. The connecting nodal line for both the stiffener element and the strip element should have the same deflection. From Eq. (A.1), the mth deflection and rotation terms of the ijth nodal line are $w^{ij}_{m} Y_m(y)\mathrm{e}^{\mathrm{i}\omega t}$ and $\theta^{ij}_{m} Y_m(y)\mathrm{e}^{\mathrm{i}\omega t}$, respectively.

Employing the same non-dimensionalization procedure as for the plate strip stiffness matrix ${}^{P}\mathbf{K}^{ij}_{mn}$ and the mass matrix ${}^{P}\mathbf{M}^{ij}_{mn}$, the non-dimensional stiffness matrix of the longitudinal stiffener placed along the ijth nodal line becomes

$$
{}^{LS}\hat{\mathbf{K}}^{ij}_{mn} = \begin{bmatrix} {}^{LS}\hat{K}^{ij}_{w,mn} & 0 \\ 0 & {}^{LS}\hat{K}^{ij}_{\theta,mn} \end{bmatrix}, \tag{A.6}
$$

where

$$
{}^{LS}\hat{K}^{ij}_{w,mn} = \frac{\eta_{2,mn}}{\pi}\omega^{j}_{LS}, \quad {}^{LS}\hat{K}^{ij}_{\theta,mn} = \frac{\eta_{1,mn}}{\pi}\tau^{j}_{LS}, \quad \omega^{j}_{LS} = \frac{\pi(EI)^{j}_{LS}}{bD}, \quad \tau^{j}_{LS} = \frac{\pi(GJ)^{j}_{LS}}{bD},
$$

and the non-dimensional mass matrix of the jth longitudinal stiffener is

$$
{}^{LS}\hat{M}^{ij}_{mn} = \begin{bmatrix} {}^{LS}\hat{M}^{ij}_{w,mn} & 0 \\ 0 & {}^{LS}\hat{M}^{ij}_{\theta,mn} \end{bmatrix}, \tag{A.7}
$$

where

$$
{}^{LS}\hat{M}^{ij}_{w,mn} = \hat{m}^{ij}_{w,LS}\eta_{0,mn}, \quad {}^{LS}\hat{M}^{ij}_{\theta,mn} = \hat{m}^{ij}_{\theta,LS}\eta_{0,mn}, \quad \hat{m}^{ij}_{w,LS} = \pi^4 \frac{(\rho A)^{j}_{LS}}{\rho h b}, \quad \hat{m}^{ij}_{\theta,LS} = \pi^4 \frac{(\rho J)^{j}_{LS}}{\rho h b^3},
$$

in which $(\rho A)^{j}_{LS}$ is the mass per unit length and $(\rho J)^{j}_{LS}$ is the torsional constant.

References

[1] C.H. Hodges, Confinement of vibration by structural irregularity, *Journal of Sound and Vibration* 82 (3) (1982) 411–424.

[2] C.H. Hodges, J. Woodhouse, Vibration isolation from irregularity in a nearly periodic structure: theory and measurements, *Journal of the Acoustical Society of America* 74 (3) (1983) 894–905.

[3] C. Pierre, M.P. Castanier, W.-J. Chen, Wave localization in multi-coupled periodic structures: application to truss beams, *American Society of Mechanical Engineers, Applied Mechanics Reviews* 49 (2) (1996) 65–86.
[4] W.-C. Xie (Guest Ed.), Special issue Dedicated to Localization Phenomenon in Physical and Engineering Sciences, *Chaos, Solitons and Fractals* 14(2) (2002).
[5] A.V. Srinivasan, Vibrations of bladed-disk assemblies—a selected survey, *Journal of Vibration, Acoustics, Stress and Reliability in Design* 106 (1984) 165–167.
[6] L.E. El-Bayoumy, A.V. Srinivasan, Influence of mistuning on rotor-blade vibrations, *American Institute of Aeronautics and Astronautics Journal* 13 (1975) 460–464.
[7] T.M. Murray, D.E. Allen, E.E. Ungar, *Steel Design Guide Series 11: Floor Vibrations Due to Human Activity*, American Institute of Steel Construction, Chicago, IL, 1997.
[8] K. Nagaya, Vibrations of cross-supported viscoelastic plates, *The Journal of the Acoustical Society of America* 61 (5) (1977) 1191–1197.
[9] J.A. Puckett, R.M. Gutkowski, Compound strip method for analysis of plate system, *American Society of Civil Engineers, Journal of Structural Engineering* 112 (1) (1986) 121–138.
[10] J.A. Puckett, G.J. Lang, Compound strip method for the free vibrational analysis of continuous rectangular plates, *American Society of Civil Engineers, Journal of Engineering Mechanics* 112 (12) (1986) 1375–1389.
[11] S. Timoshenko, S. Woinowsky-Krieger, *Theory of Shells and Plates*, 2nd Edition, McGraw-Hill, New York, 1959.
[12] Y.K. Cheung, Finite strip method in the analysis of elastic plates with two opposite ends, *Proceedings of Institution of Civil Engineers* 40 (1968) 1–7.
[13] Y.K. Cheung, *Finite Strip Method in Structural Analysis*, Pergamon Press, London, 1976.